PALEOHYDROLOGIC RECONSTRUCTION OF YAX CHEN CAVE (YUCATAN PENINSULA, MEXICO) IN RESPONSE TO HOLOCENE CLIMATE CHANGE

By
Winnie May Chan, B.A. (HONS.)

A Thesis
Submitted to the School of Geography and Earth Sciences
In Partial Fulfilment of the Requirements
for the Degree
Masters of Science

Master of Science (2017) McMaster University
(School of Geography and Earth Sciences) Hamilton, Ontario

TITLE: PALEOHYDROLOGIC RECONSTRUCTION OF YAX CHEN CAVE (YUCATAN PENINSULA, MEXICO) IN RESPONSE TO HOLOCENE CLIMATE CHANGE

AUTHOR: Winnie-May Chan
B.A. (Hons)
McMaster University
SUPERVISOR: Dr. Eduard G. Reinhardt

NUMBER OF PAGES: i, 59

ABSTRACT

Four sediment cores and ten sediment trap samples were collected from Yax Chen cave, part of the Ox Bel Ha cave system on the Yucatan Peninsula in Mexico, for microfossil and micro-XRF geochemical analysis. In cores, Cl^- trends (measuring salinity changes in meteoric water mass) show a direct relationship with microfossil (specifically the foraminifer *Elphidium* spp.) and weathering proxies (K, Ti, and Fe) used for measuring wet/dry conditions. Micro-XRF measurements of Cl^- are derived from pore water in the cores, allowing for a more accurate observation of change in the cave system. Conversely, weathering proxies are measured from transported sediments.

All four cores show a general decrease in groundwater salinity up core. Two of the cores, which were collected above the present halocline (~11m), show salinity changes in the meteoric water mass. One core was collected at the halocline and measures its movement in response to precipitation and Holocene sea-level rise. These findings are in agreement with other studies from the Yucatan coast (e.g. cenotes Aktun Ha and Sac Actum) as well as other paleoclimate records in the region. Additionally, these findings correlate with archaeological evidence, revealing several droughts that occurred throughout late Pre-Classic to late Classical Maya. High resolution analysis of Cl^- offers new insights on how coastal aquifers respond to climate change and may have implications for regional archaeology. The use of micro-XRF geochemical analysis is an effective tool which can be used to understand the spatial and temporal complexities of Yucatan coastal aquifers.

ACKNOWLEDGEMENTS

There are many individuals to thank for helping me complete my Masters of Science dissertation. First and foremost, I would like to thank Dr. Ed Reinhardt for giving me an opportunity of a lifetime to work on this project and for all the guidance and support for the past three years. Secondly, this project would not be possible without the assistance from the team in Mexico: Zero Gravity Dive Centre for providing equipment, guidance, and housing during our stay; and a huge thank you to the talented group of GUE cave divers and volunteers from the Mexico Cave Exploration Project (MCEP), for collecting the cores and sediment traps from Yax Chen.

Thank you to my colleagues at the McMaster Micropaleontology lab for assisting me with data collection and analysis in Mexico: Shawn Collins, Shawn Kovacs, Chelsi McNeil-Jewer, Anya Janzen-Krywy, Jeremy Gabriel, and Majed Turkistani.

Last but not least, I would like to thank close friends and family for all of their unconditional support throughout all these years in academia. Special mentions to Nick Riddick and Chenille Diaram for all of your encouragement and time spent on helping me edit this paper. Special thanks to Sarah and Heather Bonn who had to tolerate me for the past two years and being the most supportive roommates and friends – more importantly, thanks for the all the caffeine, wine, and pizza during dire times.

TABLE OF CONTENTS

1.0 NTRODUCTION

Mexico's Yucatan Peninsula is a low-lying carbonate platform situated between the Gulf of Mexico and the Caribbean Sea (Figure 1). It is known as a popular vacation spot for its beautiful white sand beaches, underwater recreational activities, and Mayan monuments. The Yucatan Peninsula is also the home to one of the world's most extensive underwater cave systems which formed through the dissolution of limestone by the meteoric-marine water mixing interface called the *halocline* (Beddows et al., 2007; Smart et al., 2006). Due to the high porosity and permeability of the Yucatan karst, the precipitation of rainwater percolates rapidly into the vadose zone, creating a density stratified aquifer with marine water intruding inland (Beddows et al., 2007). The karst also limits the formation of surface streams which means access to potable drinking water is limited to groundwater sources (i.e. coastal aquifers in the region) and is attainable as a result of the low-lying topography in the northern Yucatan Peninsula (Kovacs et al., 2017a). This has been the main source of drinking water for human consumption for centuries including the Ancient Maya who occupied the region since the pre-Classic around 1000 BC (Demarest, 2004). Similar to many aquifers, the groundwater in the Yucatan Peninsula is susceptible to contamination via anthropogenic pollution from the growing urbanization and industrialisation along the Riviera Maya as well as the risk of saltwater intrusion (Kovacs et al., 2017a; Alcocer et al., 1998).

The Riviera Maya (northeastern Yucatan Peninsula) is the fastest growing region in Mexico with tourism and urbanization expected to intensify up to10-fold within the next 20 years (Metcalfe et al., 2011; Hernández-Terrones et al., 2015; Alcocer et al., 1998). Presently, some of the wastewater treatment process involves a centralize sewage collection procedure where both industrial (including hotels/resorts) and domestic waste from surrounding municipalities are

pumped into the marine water mass (WM) of the aquifer. Part of the domestic waste (around 14 percent of the population) will enter inadequate wastewater treatment systems concentrated in municipal septic tanks or pit latrines (Metcalfe et al., 2011; Hernández-Terrones et al., 2015). This can increase the risk of toxins entering the aquifer via surface runoff and also contaminate the local coastal ecosystem as water discharges into the sea (Metcalfe et al., 2011; Hernández-Terrones et al., 2015).

The coast of the Riviera Maya houses the Mesoamerican Barrier reef system, the second largest coral reef in the Atlantic Ocean, which provides a wealth of oceanic biodiversity and attracts thousands of tourists to the northeastern coast of the Yucatan Peninsula annually. With the impacts of coastal pollution and rising sea surface temperatures (SSTs) in the Atlantic over the past two decades, more than 50 percent of the coral reef has been reportedly damaged (Harvell et al., 2007; Kwiatkowski et al., 2013). As anthropogenic pressures are expected to grow, it is inevitable that the tourism centered economy of the Yucatan Peninsula will be impacted in the long run. In addition, climate models predict that the Caribbean region will likely continue having higher temperatures and subsequent drier seasons for upcoming decades (Campbell et al., 2010; McLean et al., 2015; Taylor et al., 2011). Establishing a substantial understanding of how the aquifer will respond to climate trends and anthropogenic pressures is imperative for ensuring future sustainable development in the region.

There remains a lack of understanding regarding how these density stratified aquifers respond to regional and local changes. In the past, the use of foraminifera and arcellaceans (testate amoebae/thecamoebians) in the sedimentological record have been proven useful as proxies for monitoring changes in the groundwater hydrology of Yucatan caves (van Hengstum et al., 2009; Gabriel et al., 2008). Along with microfossil data, this study will offer a higher

resolution (up to 200μm) paleoenvironmental analysis using elemental data obtained via micro-X-Ray Fluoresce (μXRF) ITRAX core scanner. This non-destructive analysis is becoming an increasingly used for paleoenvironmental research (Hennekam and de Lange, 2012). This paper will provide a paleoenvironmental analysis using four cores collected in various locations along the Yax Chen cave system which is part of the larger Ox Bel Ha network in northeastern Yucatan Peninsula with over 250,000km of mapped underwater passages. Data analysis presented in this paper will concentrate on using high resolution elemental data to reconstruct salinity changes in groundwater hydrology of Yax Chen over the last ~6000 years of the Holocene through (I) examining temporal (short/long term influences); (II) spatial patterns (local/regional), and (III) examine the cave-climate relationship with existing climate records around the region. By understanding the history and complexity of these cave systems, predictive modelling can be developed to improve planning for the present and future population around the Yucatan Peninsula and related coastal environments in other parts of the world (Coutino et al., 2017). The data presented in this paper may also offer new insights for geoarchaeological research on the Classical Maya which occupied the region for centuries.

What caused the decline of the Classical Maya between ~750-870 AD remains a mystery today. Over the past decade, there have been a number of paleoenvironmental records collected in former Mayan occupied city-states all containing evidence that the region was affected by a series of multi-decadal droughts throughout the Classical Maya (Beach et al., 2016; Stahle et al., 2016; Douglas et al., 2014; Kennett et al., 2012; Hodell et al., 2005; Haug et al., 2001). As such, part of this paper will focus on comparing these existing records to the paleohydrological data from Yax Chen cave in order to understand how groundwater responded to these major changes

in regional climate and perhaps contribute to the geoarchaeological research on the ancient Maya.

1.1 *Study area*

1.1.1 *Geologic and hydrologic setting*

The Yucatan Peninsula (Figure 1) is a low-lying tectonically stable carbonate platform formed by young Holocene aged biogenic limestone and has an overlying thin layer of terra rossa soil (Bauer-Gottwein et al., 2011; Curtis et al., 1996). The karstic nature of these limestones has formed several major dissolution conduits creating Ox Bel Ha, one of the world's largest underwater cave networks, extending over 259, 909 km surveyed by cave divers (Cabadas et al., 2010; MECP, 2017). There are no surface streams or rivers found in the region as a result of the high porosity of these limestones with an average porosity ranging from 14 to 51 percent (Collins et al., 2015b; Beddows et al., 2007). As such, the Yucatan Peninsula heavily relies on their groundwater as their main source of potable drinking water.

As with many coastal karst systems, the aquifers in the region are classified as *anchialine* which are open systems with a subterranean linkage to the ocean (van Hengstum et al., 2010). Due to the high porosity and permeability of the limestones, rainwater percolates quickly and flows directly into the vadose zone of the caves. This phenomenon creates a stratified water column consisting of a warmer fresh (and sometimes slightly brackish) meteoric WM overlying the cooler denser marine WM protruding inland from the Caribbean Sea. Since these limestones have a high hydraulic conductivity, the flow in the meteoric WM is fairly low (<6cm/sec); (Collins et al., 2015a; Beddows et al., 2005). The contact between the meteoric and marine WM creates a fresh-saline mixing interface called the *halocline.* This mixing zone is responsible for

limestone dissolution forming these subaqueous anastomosing cave networks in the Yucatan Peninsula (Collins et al., 2015b; Beddows et al., 2005).

The depth of the halocline varies between locations depending on the proximity to the sea (Beddows et al., 2007). Previous studies found that caves located near the coast (e.g. Yax Chen Arizona) were reported to have stepped meteoric WM containing two haloclines whereas anchialine caves that are situated further inland (e.g. Hoyo Negro) tend to have a sharp transition between fresh-marine WMs (Kovacs et al., 2017a; Collins et al., 2015b). This is widely related to the differential turbulent movement of the outflowing meteoric water and inflowing seawater causing more mixing near the coast (Kovacs et al., 2017a; Beddows et al., 2007). The overall groundwater mixing at the halocline, however, is controlled by various regional and local scaled mechanisms including sea-level, tidal pumping, precipitation, hydrologic flow, cave morphology, and coastal plugging which is summarized in Figure 2 (Collins et al., 2015c; van Hengstum et al., 2010).

Sea-level for example, contributes to the overall height of the water table. The general position of the halocline moves up or down in response to sea-level rise or drop (Kovacs et al., 2017a). Other environmental factors including regional climate change such as, the relative position of the Intertropical Convergence Zone (ITCZ) over the Yucatan Peninsula can increase local precipitation which enforces more turbulent mixing in the cave resulting in a deeper halocline and increasing the salinity of the meteoric WM (van Hengstum et al., 2010; Kovacs et al., 2017a).

1.1.2 *Hydrologic setting of Yax Chen cave*

Yax Chen is located near the coast of the Yucatan Peninsula (~300m) and south of the ancient Mayan city of Tulum in Quintana Roo State (Figure 1). It is part of the larger Ox Bel Ha

network with ~2.7km of explored conduits and has 7 collapsed karst ceilings (known locally as *cenotes*) in its main cave line as seen in Figure 3 (Collins et al., 2015b). According to modern reconstruction of the Holocene sea-level curve in the Caribbean by Khan et al (2017), rapid eustatic sea-level rise during the Holocene would have started flooding the cave ~7500 cal. yr BP (Collins et al., 2015a). However, cave sedimentation did not begin until ~4000yBP according to radiocarbon dates obtained from sediment cores. In present day, Yax Chen is generally shallow with average water levels measuring to ~10mbsl and ~14mbsl in certain regions of the cave where there are pits on the cave floor (Collins et al., 2015b). Due to its close proximity to the Caribbean Sea, the meteoric WM tends to have a stepped halocline as seen in Kovacs et al (2017a) salinity profiles of Yax Chen's side passages *Arizona* (at depths of ~10mbsl and ~15mbsl) and *Lil Chen* (~11mbsl and ~15mbsl); (Figure 4).

1.2 *Climate*

The Yucatan Peninsula typically undergoes two major seasonality changes that are predominantly driven by the migration patterns of the Intertropical Convergence Zone (ITCZ) (Hodell et al., 2007; Alocer et al., 1998). The ITCZ is driven by SSTs and ascending atmospheric pressures (Wang et al., 2007). The average annual rainfall in the Yucatan ranges from 550-1500mm/yr, mostly occurring in the summer months (Collins et al., 2015; Bauer-Gottwein et al., 2011; Alocer et al., 1998). This wet season typically begins during the months of March/April and ends around October/November. September usually has the greatest amount of rainfall with heightened tropical storm activity (Collins et al., 2015; Hodell et al., 2005). During these months, the ITCZ migrates towards the north triggering heavy storm activity and rainfall in the region (Figure 1).

During the winter months, from October/November to March/April, the Yucatan Peninsula typically experiences dry conditions (Alocer et al., 1998). This is influenced by the ITCZ returning south towards the equator (Hodell et al., 2005). Moreover, the air temperature variation is quite low, with average temperatures typically around 25 degrees Celsius during the winter months and 28-35 degrees Celsius in the summer months (Collin et al., 2015; Hodell et al., 2007). Climate models have predicted that the Caribbean will experience warmer and drier conditions as a result of increased anthropogenic greenhouse gas emissions in the atmosphere (Taylor et al., 2011; Campbell et al., 2010). This warming and drying may add further implications to the groundwater hydrology in the Yucatan Peninsula.

1.2.1 *The Ancient Maya and paleoclimate records*

Known for their monumental cities, stone sculptures, and early scripture, the Mayan Empire flourished and ruled Mesoamerica for centuries up until their gradual decline around 750-1000 AD (Gill et al., 2007; Hodell et al., 2005). Over the past few decades, scholars have debated and argued about the controversy surrounding the possible role of climate change, namely a multi-decadal drought triggering economic, political, social, and health strains on the population leading to their downfall in the late Classical Maya (Stahle et al., 2016; Gill et al., 2007). Paleoclimate records obtained from the Cariaco Basin (Venezuela), paleolimnological studies from northern Yucatan lakes, and speleothem cave studies from Mayan city states including Belize and Guatemala, have overlapping results indicating drought events that coincide with archaeological evidence (Beach et al., 2016; Stahle et al., 2016; Douglas et al., 2014; Kennett et al., 2012; Hodell et al., 2005; Haug et al., 2001). It is, however, erroneous to argue that climate change is the sole reason for the demise of the ancient Maya. Archaeological evidence from dates recorded on monuments throughout the Yucatan Peninsula indicate that the

ancient civilization did not collapse at once, rather through three consecutive phases (Gill et al., 2007).

The three-stage collapse in the Yucatan Peninsula is divided by the periods of 761-810, 811-860, and 861-910 AD (Gill et al., 2007). The first stage of the decline (761-810AD) occurred in the southeastern coast of the Mayan empire which included cities Copán (modern day Honduras) and Caracol (Belize). The second stage (811-860 AD) saw the downfall of Aguteca (Guatemala), Palenque, and Edzná (both located in southern Yucatan Peninsula). The final stage of this reported collapse (861-910 AD) were the ancient Mayan cities, Tikal, Chichen Itza, and Uxmal that dominate the Yucatan lowlands (Gill et al., 2007). Part of the controversy with the Maya-drought debate is associated with the poor understanding of how certain city states managed to survive the droughts recorded in in the climate records. Only recently have research scientists began examining the complex hydrogeological systems in the Yucatan Peninsula to understand how the groundwater, a possible source of drinking water for the Classical Mayans, responded to the droughts.

Based on what is understood regarding the hydrogeologic setting of Yucatan coastal aquifer, the groundwater is expected to become more stratified as a result of reduced hydrologic conductivity and mixing during dry conditions (Figure 2); (Beddows et al., 2007). There is a possibility, although not definitive, that the groundwater may have had potable drinking water conditions during these droughts. Access to the groundwater would have been possible using cenotes especially for those who occupied the northern city-states in the Yucatan where the water table is much lower (Gill et al., 2007; Alcocer et al., 1998). Cenotes were important to the ancient Maya as they were used in rituals and provided some of the Mayan population with access to the aquifer for irrigation and consumption purposes (Demarest, 2004). Presently, these

sinkholes remain crucial for the development around the Yucatan Peninsula. As Quintana Roo continues to urbanize along with a growing tourist industry around the northeastern coast, the groundwater is subjected to potential risk of contamination (Kovacs et al., 2017a).

1.3 *Foraminifera and arcellaceans as indicators*

Testate Rhizopoda, foraminifera and arcellaceans (also referred to as testate amoebae/thecamoebians) are often used as proxies for documenting the impacts of climate and sea-level changes in coastal environments (van Hengstum et al., 2010; Scott et al., 2001). In more recent studies, these microfossils are proven to be useful proxies for reconstructing groundwater salinity in aquatic caves similar to Yax Chen as seen in Gabriel et al (2008) and van Hengstum et al (2008; 2011; 2012). Foraminifera and arcellaceans are single-celled protozoans that secrete their own test (shell) through autogenous processes or have an agglutinated test (xenogenous) from cementation of surrounding detritus material (Scott et al., 2001; Patterson et al., 1985). In more modern benthic samples (e.g. Holocene aged), the xenosomes are largely made up of diatom frustules (van Hengstum et al., 2007). These testate rhizopods are well preserved in the sedimentological record and are thus often used as proxies for paleoenvironmental and paleolimnological research due to their sensitivity to environmental stresses such as, changes in salinity, temperature, pH, and dissolved oxygen (Scott et al., 2001; van Hengstum et al., 2007).

Benthic foraminifera are found in environments within marine to brackish salinities whereas arcellaceans are exclusively found in freshwater environments to very low salinity with the exception of certain genus such as, *Centropyxis* that can tolerate marginally brackish salinity regimes (Farooqui et al., 2012; van Hengstum et al., 2007; Patterson and Kumar, 2002; Asioli et al., 1996). Other studies have used arcellaceans for documenting the impacts of anthropogenic

driven land alterations (i.e. pollution) in lakes and wetlands (Reinhardt et al., 1998; Patterson et al., 1985). van Hengstum et al (2008) were one of the few to first document foraminifera and arcellacean taxonomy living in cenotes Carwash, Maya Blue, and El Eden of Mexico's Yucatan Peninsula. Arcellaceans generally have low species diversity in these environments, typically dominated by the genus *Centropyxis* with the most euryhaline species *contricta "aerophilia"* and *"spinosa"* varieties capable of surviving brackish salinities around 3.3ppt (van Hengstum et al., 2008; Scott et al., 2001). Calcareous foraminifera such as *Ammonia* spp. tend to dominate the assemblages due to their wide range of salinity tolerances unlike *Elphidium* spp. which typically live in marine salinities no less than 6ppt (Scott et al., 2001). In this study, foraminifera and arcellaceans will be used along with μXRF elemental data to reconstruct the fluctuation of groundwater salinity in Yax Chen.

1.4 *Micro X-Ray florescence core scanning*

μXRF core scanning is becoming increasingly popular for various research including paleoenvironmental and sedimentological analysis. This non-destructive tool offers quick high-resolution elemental data up to 200 μm (Finné et al., 2015; Hennekam and de Lange, 2012). Most analysis is done through scanning flat surfaces of split sediment cores and requires little preparation. It is particularly useful for analyzing major elements found in the geologic record, such as silicon (Si), titanium (Ti), iron (Fe), calcium (Ca), and potassium (K). The μXRF core scanner can also detect minor elements including zinc (Zn), strontium (Sr), and barium (Ba) (Wirth and Barth, 2017). Aside from its ability to record geologic material, the μXRF core scanner can also provide real-time high resolution radiographic and optical images for further analysis (Finné et al., 2015).

In a related study to Yax Chen, Peros et al (2017) were able to perform a high resolution

paleoenvironmental analysis on three sediment cores collected from Cenote Jennifer in northern Cuba using the ITRAX μXRF core scanner. The study identified a several periods of drying and increased evaporation around 8150, 8200, and 8250 cal yr BP from large peaks of Cl^- and Br associated with the 8.2ky event which saw a drop of global atmospheric temperatures (Peros et al., 2017; Kovacs et al., 2017a). The results parallel other climate records near the region including the Cariaco Basin, $\delta^{18}O$ from ice cores in Greenland, as well as $\delta^{18}O$ results from stalagmites in Padre Cave (Brazil) and Venado Cave (Costa Rica). Another recent study conducted in the Yucatan Peninsula by Kovacs et al (2017b) used μXRF data (e.g. Cl/Ca, Sr/ Ca) on two cores from calcite raft deposits in Cenote Ich Balam and Hoyo Negro to document changes in aquifer salinity in response to Holocene climate change. In this paper, μXRF data obtained from sediment cores in Yax Chen will be used in conjunction with microfossil analysis to reconstruct paleohydrological changes. A study in Morocco by Aquit et al (2013) successfully used both μXRF data and micropaleontological analysis (benthic foraminifera) to reconstruct the facies evolution of Tarfaya Atlantic coastal basin in the Cretaceous.

2.0 METHODS

2.1 *Field*

2.1.1 *Coring*

Four sediment push cores (50 -145cm long, ~6cm diam.) were collected along the main line of the Yax Chen cave (Figure 3) providing a spatial variation to the data (i.e. upstream/downstream relationship). Each core was obtained via SCUBA techniques between the summers of 2007-2015 and was subsequently named Core (C) 2, 33, 37, and 58. Both C2 and C33 were collected at depths of ~9m (C33 being a little shallower) below the groundwater surface. C37 and C58 were obtained at depths of ~11m which is near the halocline in Yax Chen

~12-15m (see Figure 4 for salinity profiles in Yax Chen); (Kovacs et al., 2017a; Collins et al., 2015b).

2.1.2 *Sediment traps*

Collins et al (2015) used 51 sediment traps based on designs by Gardiner (1980) and placed them in 17 stations (Figure 3) along the main cave passage of Yax Chen (see Collins et al., 2015 for specific design details). The main purpose of these traps was to capture sediment influxes in Yax Chen impacted by overlying vegetation (i.e. mangrove vs. tropical forest) and cenote size. The data was originally collected annually for May 2011-12 and 2012-13, however, in order to increase the resolution of the data (i.e. capture the effects of Hurricane Ingrid on cave sedimentation), the traps were collected bi-annually every May and December since 2013. In this paper, sediment traps from May-Dec 2016 were sampled and scanned for geochemical analysis obtained via μXRF and for microfossils which is explained further in laboratory analysis.

2.2 *Laboratory analysis*

2.2.1 *μXRF analysis*

Sediment cores were split and stored in a cold room where one half was reserved for archival records and the other (working half) was used for μXRF core scanning, microfossil sampling, and radiocarbon dating (^{14}C). Samples from the sediment traps collected in December 2016 were placed into a sequential sample holder where ~1cc (1mL) of sediment was packed into sections (Gregory et al., 2017) and scanned for elements using the Cox Analytical ITRAX XRF core scanner at McMaster University Core Scanning Facility. Samples that had insufficient amount of sediment in the traps were not considered for further analysis, such as station #1. The cores and prepared samples from the sediment traps were scanned for high resolution elemental data as well as optical imagery for the cores. The cores were scanned at a 200μm resolution with

Cr tube and a count time of 15 seconds. For the purpose of this study, the μXRF core scanning results for chlorine (Cl), potassium (K), titanium (Ti), and iron (Fe) were selected for further paleoenvironmental analysis.

2.2.2 *Cl^- and salinity calculations*

This paper uses Cl^- μXRF results from the cores as a salinity proxy in Yax Chen. The equation:

$$y = 0.0019x - 0.27024$$

was used to calibrate Cl^- counts to salinity. The formula is derived from a salinity calibration curve (see Figure 5) calculated by McNeill-Jewer et al. (*submitted*) using average salinity measurements (ppt) from calcite rafts, gyttja, and mud obtained in 16 sediment cores collected around Tulum and salinity recording from water samples at the core locations using a portable handheld YSI 20 multiparameter meter (see McNeill-Jewer et al. (submitted) for more details). The formula is used to calculate paleosalinity changes in the cores, more notably for C2 in Figure 5).

2.2.3 *Microfossil analysis*

Gabriel et al. (2008) performed microfossil analysis from sampling 1cm of sediment at every 2cm of C2. C33 (2014) was sampled using 2.5cm at every 5cm intervals. C37 and C58 (2015) were sampled at higher resolutions of 0.25cm with 5cm intervals. Each sediment sample from the core and the sediment traps was washed through a 45μm sieve to remove silt and clay particles and retain the foraminifera and arcellaceans following the procedures outlined in Scott et al. (2011). Microfossils were later wet-picked and counted under an Olympus binocular dissecting microscope with 80x magnification. Scanning Electron Microscopy (SEM) imagery was performed using the SEM JEOL 6610 at the Canadian Centre for Electron Microscopy at McMaster University for taxonomy identification purposes. Foraminifera and arcellaceans

taxonomy follows previous studies in the same region covered by van Hengstum et al. (2008; 2009; 2011).

Between the samples collected from each core, a total of 15 types of foraminifera were identified with counts dominated by the calcareous and euryhaline genus *Ammonia* spp. There were three different arcellaceans identified with the genus *Centropyxis* dominating the total counts over *Arcella vulgaris* and *Difflugia* spp. Most microfossils counted in the sediment traps were mostly testate amoebae (*Centropyxis* spp.) and agglutinated species. Quantitative statistical analysis was computed sampled collected in both the core samples and sediment traps.

Relative fractional abundance of each species was calculated based on the total population of foraminifera and arcellaceans per sample (Patterson and Fishbein, 1989) following the formula:

$$F_1 = \frac{C_i}{N_i}$$

Where C_i represents the total number of one species in a sample and N_i is the total number of species in the sample (van Hengstum et al., 2008). Standard error was accounted for and applied for each sample to determine statistically significant counts using:

$$S_{Fi} = t^* \sqrt{\frac{F_i(1 - F_i)}{N_i}}$$

The t^* Represents student's t^*, F_i denotes relative fractional abundance, and N_i the total number of foraminifera and arcellaceans found in the sample (Kovacs et al., 2013; Patterson and Fishbein, 1989). Species with a standard error greater than the relative fractional abundance indicate that they are statistically insignificant and were disregarded for further multivariate analysis (Kovacs et al., 2013; Patterson and Fishbein, 1989). For example, between the five sediment cores, *Miliolid sp. A, Bolivinid* spp., *Helenina andersoni*, *Ammodiscus tenuis*, *Reophax*

catella, *Tiphotrocha comprimata,* and *Arcella vulgaris* were all removed from further statistical analysis. Q-Mode cluster analysis was performed using a micropaleontological software package called PAST (Kovacs et al., 2013). A dendrogram was produced using Ward's minimum variance with constrained incremental sum of squares (CONISS) to cluster similar samples on Euclidean distance. Species diversity and relative proportions of species were calculated using the Shannon-Weaver Diversity Index (SDI) also using PAST software. The following algorithm was used to calculate SDI:

$$SDI = -\sum_{(-)}^{s} \frac{C_i}{N_i} * In\left(\frac{C_i}{N_i}\right)$$

Variables C_i and N_i represent the same values used in the standard error calculation. Similar methods were applied for microfossil analysis in the Yax Chen May-December 2016 sediment traps. Foraminifera species found in the traps were grouped according to their test composition (i.e. calcareous and agglutinated) and arcellaceans were clustered together to see a general trend in distribution between the stations.

2.2.4 Radiocarbon Dating

Bulk organic sediment samples (gyttja) from each core were collected, pre-treated, and submitted to DirectAMS Radiocarbon Dating Service, an accelerator mass spectrometry (AMS) laboratory located in Seattle, Washington, USA (see Table 1 for sample intervals, calibrated dates, and errors).

C2 was previously sampled and described by Gabriel et al (2008) using the available organic sediment found in the core. For the pre-treatment process, sediments were washed in deionized water prior to undergoing a chemical bath containing hydrogen chloride (HCL) and

alkali (NaOH) in order to eradicate carbonate sediments and organic acids in each sample. The samples were later neutralized with acids to remove excess mechanical contaminants. Once radiocarbon results were received, they were calibrated to years before present using the Blaauw (2010) Clam package (version 2.2) for R Studio (version 1.1. 383), and age-depth models were produced for each core to supplement further analysis (Figure 6). Each age-depth model was produced using linear interpolation with a 95 percent confidence interval at every 0.02cm (200μm).

3.0 RESULTS

3.1 Microfossils in sediment traps

The microfossils recorded in the 10 sediment traps from the May-December 2016 collection period (Figure 8) show very high abundances of arcellaceans with only minor differences between the stations. The sediment traps were dominated by *Centropyxis* spp. (~50 - 70%) and agglutinated foraminifers at ~30% (*Miliammina fusca* and *Trochammina* spp.). Calcareous foraminifera including *Ammonia* spp., *Elphidium* spp., and *Ammodiscus tenuis* represent ~10% of the sample population. There was a general trend towards higher agglutinated taxa upstream which also corresponds to slightly deeper depths and salinity associated with proximity to the first halocline (Figure 3; Kovacs et al., 2017a). The meteoric WM has salinity of ~6-7ppt while the intermediate WM below the first halocline is ~15ppt and the marine WM is ~34ppt (Figure 4; Kovacs et al., 2017a).

3.2 Core Results

3.2.1 *Core Lithology and Age Depth Models*

Yax Chen sediment cores are from 55 to 145 cm in length and were predominantly homogenous comprising of rich organic material (OM, gyttja) with no significant lithological

change (Figure 7a, b). The most apparent variation is a slight colour change from light to darker laminae with variable traces of shells and carbonate sediment. The laminated bedding indicates a lack of bioturbation as would be expected in the cave environment where there are few benthic organisms. C2 however, does have a transition to more carbonate rich sediment at ~55cm.

The basal ^{14}C ages for the cores ranges from ~1300 - 3300 cal. yr BP (Figures 6, 7a,b) The age-depth models (Figure 6) show an overall near linear sediment accumulation pattern in the cores with basal ages of ~3200 cal. yr BP. C33 and C37 have mean accumulation rates of ~0.06 cm/yr and ~0.07 cm/yr) which are approximately 2X the rates found in C2 (~0.03 cm/yr) and C58 (~0.02 cm/yr). This is range of accumulation rates is likely related the proximity and size of cenotes and downstream movement of water as well as the overlying vegetation (mangrove forest versus tropical rainforest). C33 and C37 were collected near the cenote entrances of Tarpon I and II (Figure 3) which are two of the larger cenotes along the cave passage. According to Collins et al (2015), cenotes with overlying fringe mangroves tend to receive the higher sediment input since the prop roots of mangroves serve as a natural reservoir for nutrients to accrue during the wet season and enter into the cave passages via the open water cenotes with downstream flow. C2 and C58 on the contrary, are further away from cenotes and thus the sediment influx is lower.

3.2.2 *Microfossils*

The Q-mode cluster did not prove effective in discerning useful biofacies as the species diversity was low and many of the species and arcellacean strains were not identified. Scott et al. (2001) show that the proportions of arcellaceans (thecamoebians), agglutinated and hyaline foraminifera (*Ammonia* spp. and *Elphidium* spp.) are good indicators of salinity within estuaries and were used in this study. There are a total of 14 foraminifers including hyaline and

agglutinated taxa as well as arcellaceans (*Centropyxis* spp.) The hyaline species are grouped to the genus level (*Ammonia* spp., *Elphidium* spp.) and so are the arcellaceans (*Centropyxis* spp.) while the agglutinated taxa are all grouped together (Figure 6).

In all the cores, the euryhaline *Ammonia* spp. (*A. beccarii* "*tepida"* and *A. beccarii* "*parkisoniana"* varieties) dominate the microfossil record (~30 - 50%) and show little variability compared to *Elphidium* spp., *Centropyxis* spp., and agglutinated taxa. *Elphidium* spp. (~10 - 20%) are predominantly found near the base of the cores and decrease towards the top (Figure 7a and b). The opposite trends concur with the arcellacean and agglutinated taxa with a decreasing trend up core with agglutinated and then arcellaceans dominating the record. Higher abundances of agglutinated taxa represent a change in salinity to more brackish conditions (~3.5 - 6ppt) and higher dominance of *Centropyxis* spp. indicate a further reduction in salinity (van Hengstum et al., 2010). The decline in *Elphidium* spp. and increases in agglutinated taxa and then *Centropyxis* spp. is noticeable throughout all four cores and occurs consistently at ~1100 - 1200 cal yr. BP (Figure 7a,b). C2 has a drop in *Elphidium* spp. between ~2000 - 2750 cal yr. BP (40 - 55cm) which is also represented in C37 (~125 - 135cm) at a similar time period (2000 - 2500 cal yr. BP; Figures 7 a,b). In contrast to the later period (1100-1200 cal. yr BP), the drop in *Elphidium* spp. does not correspond to an increase in agglutinated taxa and *Centropyxis* spp., but in this instance, the increase is in *Ammonia* spp. and thus represents only a minor lowering of salinity.

3.2.3 *µXRF results*

The µXRF results show relationships between the terrigenous elements K, Ti, Fe with overall decreasing trends in the cores (Figure 7). C2 which is the oldest core, has a stepped change at ~2500 cal. yr BP which is partially represented in C37 where there is a change at ~2400 cal. yr BP. In C2 this corresponds to a lithologic change from more carbonate to OM rich

sediment, but in C37 there is little change. Count values from core to core are also quite variable and do not appear to follow any clear trend. For example, Ti ranges from 0.25 - 1.25, 0.1 - 0.64, 0.1 - 1.1 and 0.0 - 0.5 ($x10^3$) in C2, 33, 37 and 58 respectively. The lack of a trend likely relates to localized differences in the sources and transport pathways of terrigenous elements into the cave passages.

Cl^- shows a similar pattern as K, Ti, Fe with an overall decrease up core although it is best represented in the longer and older cores (C2 and C37). C33 shows a slight trend, while in C58 the trend up core is relatively flat (Figures 7a, b). The Cl^- counts followed predictable patterns in terms of salinity with cores taken deeper and closer to the halocline having higher Cl^- counts (Figure 11). Relationships between K, Ti, Fe and Cl^- show near logarithmic relationships with moderate R^2 values mostly between 0.3 to 0.4 (Figure 10). C58 had the poorest relationship with R^2 of only 0.01-0.08.

The average Cl^- values over the sampling interval used for microfossil analysis show direct relationships with *Elphidium* spp. The abundance (%) of *Elphidium* spp. and Cl^- show moderate to very good relationships with the R^2 ranging from 0.15 (C2) to 0.96 (C58; Figure 9). The average Cl^- counts also followed predictable patterns in terms of salinity and depth. The *Elphidium* spp. abundances did not show as distinct of a relationship although they did range higher percentages in the deeper cores and proximity to the halocline (C37 and C38). Overall, considering the data from all four cores, there was a general trend towards higher Cl^- and *Elphidium* spp. abundance with proximity to the halocline and the marine WM (Figure 9).

4.0 DISCUSSION

4.1 Distribution of microfossils in Yax Chen

As documented in the sediment traps (Figure 8), the inter-station variability of foraminifera (hyaline and agglutinated taxa) and arcellaceans is generally low, with arcellaceans being significantly more abundant (>50 percent) than the foraminifers per sample which is high relative to the salinity of the meteoric WM which is ~6ppt and as high as 9ppt during large rainfall events when more mixing with the marine WM occurs (Kovacs et al., 2017a). This salinity regime is more suitable for agglutinated and hyaline foraminifera such as *Ammonia* spp. and *Elphidium* spp. (>3.7ppt, van Hengstum et al., 2008; > 6ppt, Scott et al., 2001; Millar et al., 1982) rather than arcellaceans (<3.4ppt). The agglutinated taxa are abundant in the sediment trap samples (~10 - 30%) but the calcareous taxa are not (<10%) and the higher arcellacean abundance (60-80%) is more fitting with salinity <3ppt based on van Hengstum et al. (2008). There may be other environmental variables contributing to the distribution of foraminifera and arcellacens in Yax Chen (e.g. oxygenation or short-term salinity changes), but the very high arcellaceans abundance suggests taphonomic biases with transport. As discussed in Collins et al. (2015c), OM is transported into the cave passages via the karst windows or sunlit cenotes where primary productivity occurs. It is likely that the small and light arcellacean tests are also transported into the cave with flocs of OM, perhaps originating in the wetlands/mangroves surrounding the cenotes. Abundant diatoms are also found in the sediment samples also indicating this mode of transport. Babalola et al. (2013) found riverine transported arcellaceans in Holocene cores from brackish marine inlets from British Columbia so the phenomena is not uncommon. Therefore, the larger and heavier calcareous and agglutinated taxa are likely the biocenosis although it is possible that some *Centropyxis* spp. are part of the living assemblage as

well. Nonetheless, changes in *Elphidium* spp. and agglutinated taxa abundance does predict salinity changes while *Ammonia s*pp. will be less useful as it is notably euryhaline (van Hengstum et al., 2008; Scott et al., 2001).

4.2 Relationships between microfossils and elemental records

4.2.1 Microfossils

There are good relationships between pore-water Cl^- and *Elphidium* spp. from the cores. Each core record shows a direct relationship with increasing Cl^- counts and *Elphidium* spp. abundance. The R^2 is better in some cores versus others, but there is an overall tendency towards higher *Elphidium* spp. and Cl^- counts with all the core data. The spread in the data and the variable R^2s are due to sampling resolution and proxy sensitivity to environmental change. The microfossils are time averaged over 1.0 - 0.5cm sampling intervals which represents several years to decades of time. The Cl^- data is at 0.2mm resolution and quite variable at different points in the cores, but for comparison, the data is also averaged over the same intervals. The spread in the data is likely due to the response of the microfossils to salinity changes. Kovacs et al. (2017a) showed that large rainfall events caused short-term salinity changes (1- 3 weeks) in the meteoric WM associated with entrainment of saline water from the underlying marine WM. Such short-term changes in salinity will not be recorded by the foraminifera/arcellaceans since it would take time for a new fauna to replace the old community. Foraminifera and arcellaceans also have been known to encyst themselves to survive short-term environmental changes (Scott et al., 2001, Patterson et al., 1997). Many of these taxa are also somewhat, or largely euryhaline and can exist in a range of salinities (esp. *Ammonia* spp.). The Cl^- data however, record immediate changes in WM salinity which is then entrapped in pore space within the sediment and OM, so comparisons between proxies with differing sensitivities will create some spread in

the data. There is however, as stated, a general trend between *Elphidium* spp. and Cl^- which is also shown with cores closer to halocline. The deeper cores have higher Cl^- counts versus the shallower cores as they are closer to the mixing zone between the meteoric and marine WMs. The *Elphidium* spp. abundance however, are not as well defined, there is a slight tendency to higher *Elphidium* spp. abundance with proximity to the halocline but it is not as well defined as with Cl^-. This is likely due to the sensitivity of *Elphidium* spp. to salinity and its euryhaline ecological range (Scott et al., 2001). There also could be other influences such as, substrate or oxygenation which can play a part. Therefore, the microfossil records are useful for defining overall trends, but do not resolve short-term and small changes in salinity of the meteoric WM like the Cl^- records. However, this approach integrating μXRF data with other proxies is nonetheless important, as it allows independent vetting of the elemental data (e.g. Peros et al., 2017)

4.2.2 *Elemental records*

In all the cores, Cl^- shows a good relationship between the terrigenous/weathering proxies (sediment and oxyhydroxides), K, Ti, and Fe with values ranging from 0.01 to 0.44 (Figure 10). A logarithmic trend line for each core was calculated for a best-fit curve showing a relationship between K, Ti, and Fe with Cl^- that decreases in higher counts. The relationship between these elements is variable among the cores which may be related to spatial factors including, proximity to the cenote, the size of the cenote, and the type of overlying vegetation that controls sediment accumulation in Yax Chen (Collins et al., 2015b). The poor relationship between K, Ti, and Fe with higher values of Cl^- is probably associated with the sensitivity of the elemental proxies (Rothwell and Croudace, 2015). The nature of these elements along with the varying depositional environment (i.e. sediment accumulation) possibly contribute to data

variability (Figure 10). Cl^- is recording pore-water and thus immediate responses with precipitation and mixing between the meteoric and marine WM. K, Ti, and Fe, in contrast, are recoded mainly in sediment and oxyhydroxides produced through limestone weathering which are then transported into the cave. It could be that with wetter and more frequent rainfalls weathering reaches a stasis in terms of limestone dissolution and then transport into the cave making it less sensitive during very wet conditions. Cl^- however, is responding immediately to mixing between the meteoric and marine WM throughout the shift in precipitation (i.e. a liner response). The very poor relationship in C58 is likely due to complications with sediment flux as this core location is very close to the halocline at (~11m). Observations during dives found that light flocs of OM tend to be in higher concentration in the meteoric WM versus the marine WM due to density stratification. Despite these complications with terrigenous element sensitivity, the overall trend with Cl^- indicates that with increased weathering and thus precipitation, the meteoric WM salinity is also increasing which matches instrumental records of WM dynamics during large rainfall events (Kovacs et al., 2015a).

4.3 Cl^- Core Records and their Hydrologic Implications

The core records for the last ~2 ka are ~1m in length and sea-level rise estimates are <1m for the last ~ 2000 years (Khan et al. 2017). Water depth has thus remained relatively constant at any given location during the accumulation period of the cores. Therefore, the Cl^- records should only be recording movements of the halocline and flow in the meteoric WM and mixing. Many paleoclimate records show an overall drying trend in the Caribbean during the last ~2000 years with droughts often cited as causing the decline of the Classic Maya and we would expect some effect on the groundwater (Figure 13; e.g. (Beach et al., 2016; Stahle et al., 2016; Douglas et al., 2014; Kennett et al., 2012; Hodell et al., 2005; Haug et al., 2001).

Cl^- shows an overall decreasing trend towards the top of each core except in C58 where it is relatively unchanged (Figure 11). As discussed, the magnitude of the Cl^- counts are reflected in the core position relative to the modern halocline with shallower cores having lower counts versus deeper cores. The salinity of the meteoric water at any given depth is a reflection of proximity to the halocline and mixing between the meteoric and marine WM and also localized effects associated with that mixing process including cave passage shape, diameter, wall roughness, and obstructions to flow (i.e. hydraulic jumps - limestone breakdown on the cave bottom; van Hengstum et al., 2010). This will create spatial and temporal differences in salinity at any given location relative to the position of the halocline and flow patterns in the meteoric WM especially associated with the amounts and rates of precipitation (Kovacs et al., 2017a). However, relative changes should be discerned in the salinity records associated with wet and dry periods and the mixing process through entrainment of marine water into the meteoric WM. The salinity being recorded at any given location will depend on movement of the halocline, meteoric WM flow, and as discussed sediment accumulation and sea-level change (Figure 12).

During dry periods the halocline should be shallower in depth and flows in the meteoric WM should be lower relative to wet periods (Figure 12). The expectation is that during dry periods, the meteoric WM would be less saline and the volume of water would be less, while during wet periods the volume would be larger but more saline (Kovacs et al., 2017b). Complicating this model is coastal plugging or occlusion of coastal karst limestone with cements and sediment with deceleration of Holocene sea-level rise (Ward, 2004; van Hengstum et al., 2010; Ward and Brady, 1979). This process may have created a natural damming of the aquifer stabilizing the hydraulic conductivity in the meteoric WM resulting in less turbulent mixing and overall drainage of meteoritic water (Figure 2; van Hengstum et al., 2010; Vacher and Wallis,

1992; Vacher et al. 2002; Perry et al., 1989). As speculated in van Hengstum et al. (2010) this may cause a thicker fresher meteoric WM, however, there is very little data to substantiate or gauge its effect.

4.3.1 *C37 and C58*

C37 (~10.3m) and C58 (~11m) were collected in deeper portions of the cave and closer to the halocline (~11m; Figure 3). C58 is the only core that does not show a decreasing trend in salinity up core (Figure 11). There is a transition from high to low Cl^- variability in both cores at ~900-1000 AD which correlates with the reduction in *Elphidium* spp. (1100-1200 cal yr BP). C58 which is presently close to the halocline would be expected to have a trend towards elevated Cl^- records with movement of the halocline upwards with a drying trend. The change in variability at ~900-1000 AD indicates that there was a change in the hydrology with less precipitation events and/or the halocline is getting deeper (Kovacs et al., 2017). C37 which is slightly shallower and further away from the halocline (~0.8m) shows a similar trend with higher Cl^- variability prior to 900 - 1000 AD but the values are also higher and show an overall freshening trend. This indicates an overall movement of the halocline downward and reduced meteoric WM salinity as the location gets further away from the halocline and/or there is less precipitation and mixing. If the halocline was getting shallower with overall drying trends, the Cl^- counts would be higher, however, they are not. For that reason, coastal plugging must be contributing by ponding meteoric water and reducing flows as well.

4.3.2 *C2 and C33*

C2 and C33 both show clear decreasing trends in Cl^- over the last ~2 Ka. The Cl^- counts are similar in terms of magnitude (6-8 $x10^3$) and are commensurate with their depth (~9.1m) and position relative to the halocline (i.e. C37 and C58). The reduction in *Elphidium* spp. (1100-1200

cal. yr BP) is also occurring at the same time in both cores indicating lower salinity associated with thickening of the meteoric WM and reduced flows with less precipitation. However, there is also low-amplitude variation in the Cl^- records that does not correlate well between C2 and C33.

C33 was collected very close to Tarpon 1 and only ~ 5 m downstream into the cave where the passage is restricted with low ceiling height (3 - 4m). Mangrove also surrounds Tarpon 2, and inflows of less saline mangrove water during precipitation events maybe affecting the Cl^- record in this location (Collins et al., 2015b, Kovacs et al., 2017a). The ^{14}C age model in C33 is also affected by some reworking of OM with older dates at the top of the core making it less reliable. C2 was collected further downstream from Tarpon 2 and in a very large portion of the cave passage with high ceilings (4 - 5m). The ^{14}C age model was also very good in terms of age chronology and it spans the longest time period of all the cores (~ 3.5 ka). Its depth (~ 9.1m) relative to the halocline (~11m) also makes it the best core to document short-term changes in meteoric WM salinity as it further away from the halocline and the mixing zone.

4.4 *Linkage with paleoclimate records*

4.4.1 *Paleohydrological records*

The Cl^- record from C2 shares similarities to other paleohydrologic records. Similar studies in Aktun Ha a nearby and separate cave system further in land (~8.5 kms from the coast) shows overall decreasing meteoric WM salinity over the last ~4 ka that matches the Yax Chen record. The proxies including arcellaceans and foraminifera which showed an overall decreasing salinity with a noted decrease during the Classic Mayan droughts (van Hengstum et al., 2010). The resolution of the record however, was affected by irregular and low sediment accumulation rates. Hoyo Negro from the Sac Actun cave system spans a longer time period (~8.5 Ka) and is also further inland as Aktun Ha. The study used Cl^- records from calcite rafts that record the

very upper surface of the meteoric WM (Kovacs et al., 2010b). The results showed gradually decreasing salinity of the meteoric WM spanning the past ~7 ka which matches Aktun Ha and also now Yax Chen. The agreement between the proxy records and in different cave systems indicates that a least regionally, the aquifer is responding to changes in climate (wet and dry) and also karst geomorphology with coastal plugging at the coast.

4.4.2 *Lake and speleothem records and the Classic Mayan droughts*

C2 shows long-term but also short-term trends in meteoric WM salinity (Cl^-) that correlate well with lake and speleothem records from the Yucatan and the Caribbean. Pac Chen, Chichancanab, and Punta Laguna lake records all show increased aridity in the Late to Terminal Classic period which is also recorded in the Yok Balum (Belize) and Tecoh speleothem (Figure 13; Beach et al., 2016; Stahle et al., 2016; Douglas et al., 2014; Kennett et al., 2012; Hodell et al., 2005; Haug et al., 2001). There are five phases of reduced flow in the meteoric WM and subsequent reduced salinity found in the C2 record. These include i) 900 - 1000 AD and ii) 800 - 850 AD which are associated with the Late to Terminal Classic droughts and also recorded in Pac Chen, Punta Laguna, and Chichancanab in terms of timing and periodicity. The Tecoh and Yok Balum speleothem do show periods of aridity, but the timing is slightly offset compared to the Yax Chen record. iii) 500 - 600 AD is a slight decrease in salinity but corresponds with the Mayan Hiatus (530-590 AD; Gill et al., 2007) which is represented in the Tecoh speleothem and some of the other records but these events are slightly offset in timing perhaps due to dating issues (i.e. Chichancanab and Punta Laguna) iv) 400-450 AD is only represented in the Tecoh speleothem but not in any of the other proxy records. v) 150 - 250 is represented in Pac Chen and Yok Balum but not in the other records and spans the Pre-Classic Abandonment (150-200 AD; Gill et al., 2007).

The correspondence between these independent records of aridity and reduced salinity of the meteoric WM in Yax Chen shows that the aquifer is responsive to short-term changes in rainfall. Reduced precipitation and flows in the meteoric WM towards the coast are causing less entrainment of marine water and thus a less saline aquifer during periods of drought (Kovacs et al., 2017a). These short-term trends are overprinted with a general freshening of the aquifer associated with a long-term reduction in precipitation and also coastal plugging. This is causing the aquifer to become less-saline, but also larger in volume as the meteoric WM is getting thicker. This has important implications for understanding the Classic Maya decline especially in the northern lowlands where the groundwater is more accessible due to topography (Beach et al., 2016). Counterintuitively during droughts, the aquifer is becoming more potable versus wet periods where mixing with marine water would cause elevated salinity. Further research is required to understand the temporal and spatial patterns which may be quite different, however, this study does indicate that aquifer is responding to climate change and these paleohydrological records can be important for understanding long-term interactions which are not possible with instrumental studies.

5.0 CONCLUSION

The paleohydrologic record obtained from the sediment cores in Yax Chen reinforces the studies conducted by van Hengstum et al. (2010) and Kovacs et al. (2017a, b), providing higher resolution data. The Cl^- μXRF record is proven to be a reliable proxy for salinity and it is able to capture both long-term (e.g. coastal plugging) and short-term (e.g. precipitation) events that cannot be achieved using micropaleontological analysis alone. There is a clear relationship between precipitation and the salinity of the aquifer. During dry periods the aquifer is less saline due to reduced mixing with the underlying marine WM. Coastal plugging due to deceleration of

sea-level rise also seems to be having an effect causing increased stratification but also a thicker meteoric WM. Further research is required to understand the spatial and temporal changes in the Yucatan, but this study indicates that sediment archives within the cave systems can be a useful record of aquifer change that has yet to be fully explored or understood, but has important implications for understanding the Classic Mayan droughts but also future impacts of climate and sea-level change in anchialine aquifers in the Yucatan but also elsewhere in the world.

6.0 REFERENCES

Alcocer, J., Lugo, A., Marín., L. E., and Escobar, E. (1998). Hydrochemistry of waters from five cenotes and evaluation of their suitability for drinking-water supplies, northeastern Yucatan, Mexico. *Hydrogeological Journal* **6**, 293-301.

Asioli, A., Medioli, F. S., and Patterson, R. T. (1996). Thecamoebians as a tool for reconstruction of paleoenvironments in some Italian lakes in the foothills of the southern Alps (Orta, Varese and Candia). *Journal of Foraminiferal Research* **26** (3), 248-263. Pages Magazine 24 (2), 66-67.

Aquit, M., Kuhnt, W., Holbourn, A., Chellai, E. H., Stattegger, K., Kluth, O., and Jabour, H. (2013). Late Cretaceous paleoenvironmental evolution of the Tarfaya Atlantic coastal Basin, SW Morocco. *Cretaceous Research* **45**, 288-305.

Babalola, L., Patterson, R. T., and Prokoph, A. (2013). Foraminiferal evidence of late Holocene westward shift of the Aleutian low pressure system. *The Journal of Foraminiferal Research* **143**, 127-142.

Bauer-Gottwein, P., Gondwe, B. R. N., Charvet, G., Marín, L. E., Rebolledo-Vieyra, M., and Merediz-Alonso, G. (2011). Review: The Yucatan Peninsula karst aquifer, Mexico. *Hydrogeology Journal* **19**, 507-524.

Beach, T., Luzzadder-Beach, S., Dunning, N., and Cook, D. (2016). Climatic changes and collapses in Maya History. *Pages Magazine* **24** (2), 66-67.

Beddows, P. A., Smart, P. L., Whitaker, F. F., and Smith, S. L. (2007). Decoupled fresh-saline groundwater circulation of a coastal carbonate aquifer: Spatial patterns of temperature and specific electrical conductivity. *Journal of Hydrology* **346**, 18-32.

Beddows, P. A., Smart, P. L., Whitaker, F. F., and Smith, S. L. (2005). Density Stratified Groundwater circulation on the Caribbean Coast of the Yucatan Peninsula, Mexico. *Karst Waters Institute Special Publication* **7**, 129-134.

Cabadas, H. V., Solleiro, E., Sedov, S., Pi., T., and Alcala. (2010). The Complex Genesis of Red Soils in Peninsula de Yucatan, Mexico: Minerological, Micromorphological, and Geochemical Proxies. *Eurasian Soil Science* **43** (33), 1439-1457.

Campbell, J. D., Taylor, M. A., Stephenson, T. S., Watson, R. A., and Whyte, F. S. (2010). Future climate of the Caribbean from a regional climate model. *International Journal of Climatology* **31** (12), 1866-1878.

Chagué-Goff, C., Chan, J. C. H., Goff, J., and Gadd, P. (2016). Late Holocene record of environmental changes, cyclones and tsunamis in a coastal lake, Mangaia, Cook Islands. *Island Arc* **25**, 333-349.

Collins, S. V., Reinhardt, E. G., Rissolo, D., Chatters, J. C., Nave Blank, A., and Luna Ereguerena, P. (2015a). Reconstructing water level in Hoyo Negro, Quintana Roo, Mexico, implications for early Paleoamerican and faunal access. *Quaternary Science Reviews* **124**, 68-83.

Collins, S. V., Reinhardt, E. G., Werner, C. L., Le Maillot, C., Devos, F., Meacham, S. S. (2015b). Regional response of the coastal aquifer to Hurricane Ingrid and sedimentation flux in the Yax Chen cave system (Ox Bel Ha) Yucatan, Mexico. *Paleogeography, Palaeoclimatology, Paleoecology* **428**, 226-238.

Collins, S. V., Reinhardt, E. G., Werner, C. L., Le Maillot, C., Devos, F., and Rissolo, D. (2015c). Late Holocene mangrove development and onset of sedimentation in Yax Chen

cave system (Ox Bel Ha) Yucatan, Mexico: implications for using cave sediments as a sea-level indicator. *Paleogeography, Paleoclimatology, Paleoecology* **438**, 124-134.

Coutino, A., Stastna, M., Kovacs, S. E., Reinhardt, E. G. (2017). Hurricames Ingrid and Manuel (2013) and their impact on the salinity of the Meteoric Water Mass, Quintana Roo, Mexico. *Journal of Hydrology* **551**, 715-729.

Croudace, I. W., and Rothway, R. G. (2015). *Micro-XRF Studies of Sediment Cores: Applications of a non-destructive tool for the environmental sciences*. New York / London: Springer Dordrecht Heidelberg.

Curtis, J. H., Hodell, D. A., and Brenner, M. (1996). Climate Variability on the Yucatan Peninsula (Mexico) during the Past 3500 Years, and Implications for Maya Cultural Evolution. *Quaternary Research* **46**, 37.

Demarest, A. (2004). *Ancient Maya: the Rise and Fall of a Rainforest Civilization*. New York: Cambridge University Press.

Douglas, P. M. J., Pagnani, M., Canuto, M. A., Brenner, M., Hodell, D. A., Eglinton, T. I., and Curtis, J. H. (2014). Drought, agricultural adaptation, and sociopolitical collapse in the Maya lowlands. *PNAS* **112** (18), 5607-5612.

Farooqui, A., Kumar, A., Swindles, G. T. (2012). Thecamoebian communities as proxies of seasonality in lake Sadatal in the Ganga-Yamuna Plains of North India. *Palaeontologia Electonica* **15** (1), 2-19.

Finné, M., Kylander, M., Boyd, M., Sundqvist, H. S., and Löwemark, L. (2015). Can XRF scanning of speleothems be used as a non-destructive method to identify paleoflood events in caves? *International Journal of Speleology* **44** (1), 17-23.

Gabriel, J. J., Reinhardt, E. G., van Hengstum, P. J., and Beddows, P. A. (2008). Late Holocene (3500 yBP) salinity changes and their climatic implications as recorded in an anchialine cave system, Ox Bel Ha, Yucatan, Mexico. (Unpublished Master's thesis). McMaster University, Hamilton, ON, Canada.

Gabriel, J. J., Reinhardt, E. G., Peros, M. C., Davidson, D. E., van Hengstum, P. J., and Beddows, P. A. (2008). Paleoenvironmental evolution of Cenote Aktun Ha (Carwash) on the Yucatan Peninsula, Mexico and its response to Holocene sea-level rise. *Journal of Paleolimnology* **42**, 199-213.

Gill, R. B., Mayewski, P. A., Nyberg, J., Haug, G. H., and Peterson, L. C. (2007). Drought and the Maya Collapse. *Ancient Mesoamerica* **18**, 283-302.

Gregory, R. B., Reinhardt, E. G., Macumber. A. L. Nasser, N. A., Patterson. R. T., Kovacs, S. E., and Galloway, J. M. (2017). *Journal of Paleolimnology* **57**, 287-293.

Harvell, D., Jordan-Dahlgren, E., Merkel, S., Resenberg, E., Raymundo, L., Smith, G., Weil, E., and Willis, B. (2007). Coral diseases, environmental drivers, and the balance between coral and microbial associates. *Oceanography* **20**, 172-195.

Haug, G. H., Hughen, K. A., Sigman, D. M., Peterson, L. C., and Röhl, U. (2001). Southward Migration of the Intertropical Convergence Zone through the Holocene. *Science* **293**, 1304-1308.

Hennekam, R., and de Lange, G. (2012). X-ray fluorescence core scanning of wet marine sediments: methods to improve quality and reproducibility of high resolution paleoenvironmental records. *Limnology and Oceanography: Methods* **10**, 991-1003.

Hernández-Terrones, L . M., Null, K. A., Ortega-Camacho, D., and Paytan, A. (2015). Water quality assessment in the Mexican Caribbean: Impacts on the coastal ecosystem. *Continental Shelf Research* **102**, 62-72.

Hodell, D. A., Brenner, M., and Curtis, J. H. (2005). Terminal Classic drought in the northern Maya lowlands from multiple sediment cores in Lake Chichancanab (Mexico). *Quaternary Science Reviews* **24**, 1413-1427.

Hodell, D. A., Brenner, M., Curtis, J. H., Medina-González, R., Can, E. I.C., Albornaz-Pat, A, and Guilderson, T. P. (2005). Climate change on the Yucatan Peninsula during the Little Ice Age. *Quaternary Research* **63**, 109-121.

Hodell, D. A., Brenner, M.m Curtis, J. H., and Guilderson, T. (2001). Solar Forcing of Drought Frequency in the Maya Lowlands. *Science* **292**, 1367-1370.

Jorissen, F. J., Fontanier, C., and Thomas, Ellen. (2007). Paleooceanographical proxies based on deep-sea benthic foraminifera assemblage characteristics. *Developments in Marine Geology* **1**, 263-313.

Kennett, D. J., Breitenbach, S. F. M., Aquino, V. V., Asmerom, Y., Awe, J., Baldini, J. U. L., Bartlein, P., Culleton, B. J., Ebert, C., Jazwa, C., Macri, M. J., Marwan, N., Polyak, V., Prufer, K. M., Ridley, H. E., Sodemann, H., Winterhalder, B., and Haug, G. H. (2012). Development and disintegration of Maya political systems in response to climate change. *Science* **338**, 788-791.

Khan, N. S., Ashe, E., Horton, B. P., Dutton, A., Kopp, R. E., Brocard, G., Engelhart, S. E., Hill, D. E., Peltier, W. R., Vane, C. H., and Scatena, F. N. (2017). Drivers of Holocene sea-level change in the Caribbean. *Quaternary Science Reviews* **155**, 13-36.

Kwiatkowski, L., Cox, P. M., Economou, T., Halloran, P. R., Mumby, P. J., Booth, B. B. B., Carilli, J., and Gunzman, H. M. (2013). Caribbean coral growth influenced by anthropogenic aerosol emissions. *Nature Geoscience* **6**, 362-366.

Kovacs, S. E., Reinhardt, E. G., Stastna, M., Coutino, A., Werner, C., Collins, S. V., Devos, F., and Le Maillot, C. (2015a). Hurricane Ingrid and Tropical Storm Hanna's effects on the salinity of the coastal aquifer, Quintana Roo, Mexico. *Journal of Hydrology* **551**, 703-417.

Kovacs, S. E., Reinhardt, E. G., Chatters, J. C., Rissolo, D., Schwartz, H. P., Collins, S. V., Kim, S. T., Blank, A. N., Erreguerena, P. L. (2017b). Calcite raft geochemistry as a hydrological proxy for Holocene aquifer conditions in Hoyo Negro and Ich Balam (Sac Actun Cave System), Quintana Roo, Mexico. *Quaternary Science Reviews* (in press).

Kovacs, S. E., van Hengstum, P. J., Reinhardt, E. G., Donnelly, J. P., and Albury, N. A. (2013). Late Holocene sedimentation and hydrologic development in a shallow coastal sinkhole on Great Abaco Island, The Bahamas. *Quaternary International* **317**, 118-132.

Masson, M. A. (2012). Maya collapse cycles. *Proceedings of the National Academy of Science* **109** (45), 18237-18238.

Medina-Elizalde, M., Burns, S. J., Lea, D. W., Asmerom, Y., von Gunten, L., Polyak, V., Vuille, M., and Karmalkar, A. (2010). High resolution stalagmite climate record from the Yucatán Peninsula spanning the Maya terminal classic period. *Earth and Planetary Science Letters* **298**, 255-262.

Metcalfe, C. D., Beddows, P. A., Gold-Bouchot, G., Metcalfe, T. L., Li, H., and van Lavieren, H. (2011). Contaminants in the costal karst aquifer system along the Caribbean coast of the Yucatan Peninsula, Mexico. *Environmental Pollution* **159**, 991-997.

Mexico Cave Exploration Project. (2017). Ox Bel Ha. Retrieved from http://www.mcep.org.mx/ox-bel-ha.html

McCrone, A. W. and Schafer, C. (1966). Geochemical and sedimentary environments of foraminifera in the Hudson River estuary, New York. *The Micropaleontology Project Incorporated* **12** (4), 505-509.

McLean, N. M., Stephenson, T. S., Taylor, M., A., and Campbell, J. D. (2015). Characterization of future Caribbean rainfall and temperature extremes across rainfall zones. Advances in *Meterology* **2015**, 1-18.

McNeill-Jewer, C. A., Reinhardt, E. G., Krywy-Janzen, A., Coutino, A., Stastna, M., Rissolo, D., Meacham, S. (2017). *Salinity changes during the Mayan droughts documented through pore water chlorine in sediment cores from Quintana Roo, Mexico*. Manuscriot submitted for publication

Millar, A. A. L., Mudie, P. J., and Scott, D. B. (1982). Holocene history of Bedford Basin, Nova Scotia: foraminifera, dinoflagellate and pollen records. *Canadian Journal of Earth Sciences* **19**, 2342-2367.

Munro, P. G. and Zurita, M. D. L. (2011). The role of cenotes in the social history of Mexico's Yucatan Peninsula. *Environment and History* **17**, 583-612.

National Hurricane Centre. (2016). *Hurricane Earl*. Retrieved from http://www.nhc.noaa.gov/archive/2016/al05/al052016.public.007.shtml?

Patterson, R. T., and Kumar, A. (2002). A Review of current testate rhizopod (thecamoebian) research in Canada. *Palaeogeography, Palaeoclimatology, Palaeoecology* **180** (1-3), 225-251.

Patterson, R.T., McKillop, W.B., Kroker, S., Nielsen, E., and Reinhardt, E.G. (1997). Evidence for rapid avian-mediated foraminiferal colonization of Lake Winnipegosis, Manitoba, during the Holocene Hypsithermal. *Journal of Paleolimnology* **18**, 131–143.

Patterson, R. T., MacKinnon, K. D., Scott, D. B., and Medioli, F. S. (1985). Arcellaceans ("Thecamoebians") in small lakes of New Brunswick and Nova Scotia: modern distribution and Holocene stratigraphic changes. *Journal of Foraminiferal Research* **15**, 114-137.

Peros, M., Collins, S., G'Meiner, A. A., Reinhardt, E. G., and Pupo, F. M. (2017). Multistage 8.2 kyr event revealed through high-resolution XRF core scanning of Cuban sinkhole sediments. *Geophysical Research Letters*, 1-9.

Perry, E., Paytan, A., Pedersen, B., Velazquez-Oliman, G. (2009). Groundwater geochemistry of the Yucatan Peninsula, Mexico: Constraints on stratigraphy and hydrogeology. *Journal of Hydrology* **367**, 27-40.

Perry, E., Velazquez-Oliman, G., and Marin, L. (2002). The hydrogeochemistry of the Karst Aquifer System of the Northern Yucatan Peninsula, Mexico. *International Geology Reviews* **44**, 191-221.

Perry, E., Swift, J., Gamboa, J., Reeve, A., Sanborn, R., Marin, L., and Villasuso, M. (1989). Geologic and environmental aspects of surface cementation north coast, Yucatan, Mexico. *Geology* **17** (19), 818-821.

Reinhardt, E. G., Dalby, A. P., Kumar, A., and Patterson, R. T. (1998). Arcellations as Pollution indicators in Mine Tailing Contaminated Lakes near Colbalt, Ontario, Canada. *Micropaleontology* **44** (2), 131-148.

Rothwell, G., and Croudace, I. W. (2015). Twenty Years of XRF Core Scanning Marine Sediments: What Do Geochemical Proxies Tell Us?, *Micro-XRF Studies of Sediment Cores: Applications of a non-destructive tool for the environmental sciences*. London: Springer.

Scott, D. B., Medioli, F. S., Schafer, C. T. (2001). *Monitoring in Coastal Environments Using Foraminifera and Thecamoebian Indicators*. Cambridge University Press, Cambridge, United Kingdom.

Smart, P. L., Beddows, P. A., Coke, J., Doerr, S., Smith, S., and Whitaker, F. F. (2006). Cave Development on the Caribbean coast of the Yucatan Peninsula, Quintana Roo, Mexico. Geological Society of America 404, 105-128.

Stahle, D. W., Cook., E. R., Burnette, D. J., Villanueva, J., Cerano, J., Burns, J. N., Griffin, D., Cook, B, I., Acuña., Toberson, M. C. A., Szejner, P., Howard, I. M. (2016). The Mexican Drought Atlas: Tree-ring reconstructions of the soil moisture balance during the late pre-Hispanic, Colonial, and modern eras. *Quaternary Science Reviews* **149**, 34-60.

Taylor, M. A., Stephenson, T. S., Owino, A., Chen, A. A., Campbell, J. D. (2011). Tropical gradient influences on Caribbean rainfall. *Journal of Geophysical Research: Atmospheres* **116**, 1-14.

Toscano, M. A. and Macintyre, I. G. (2003). Corrected western Atlantic sea-level curve for the last 11,000 years based on calibrated ^{14}C from *Acropora palmate* framework and intertidal mangrove peat. *Coral Reefs* **22**, 257-270.

Vacher, H.L. and Mylroie, J.E. (2002). Eogenetic karst from the perspective of an equivalent porous medium. *Carbonates and Evaporites* **17** (2), 182-196.

Vacher, H. L. and Wallis, T. N. (1992). Comparative Hydrogeology of Fresh-Water Lenses of Bermuda and Great Exuma Island, Bahamas. *Groundwater* **30** (1), 15-20.

van Hengstum, P.J., and Scott, D. B. (2012). Sea-level rise and coastal circulation controlled Holocene groundwater development in Bemuda and caused a meteoric lens to collapse 1600 years ago. *Marine Micropaleontology* **90-91**, 29-43.

van Hengstum, P.J., and Scott, D. B. (2011). Ecology of foraminifera and habitat variability in an underwater cave: distinguishing anchialine versus submarine cave environments. *Journal of Foraminiferal Research* **41** (3), 201-229.

van Hengstum, P. J., Scott, D. B., Gröcke, D. R., and Charette, M. A. (2011). Sea level controls sedimentation and environments in coastal caves and sinkholes. *Marine Geology* **286**, 35-50.

van Hensgtum, P.J., Reinhardt., E. G., Beddows, P. A., and Gabriel, J. J. (2010). Linkages between Holocene paleoclimate and paleohydrogeology preserved in a Yucatan underwater cave. *Quaternary Science Reviews* **29**, 27888-2798.

van Hengstum, P. J., Reinhardt, E. G., Beddows, P. A., Schwarcz, and Gabriel, J. J. (2009). Foraminifera and testate amoebae (thecamoebians) in an anchialine cave: surface distributions from Aktun Ha (Carwash) cave system, Mexico. *Limnology and Oceanography* **54** (1), 391-396.

van Hengstum, P. J., Reinhardt, E. G., Beddows, P. A., Huang, R. J., and Gabriel, J. J. (2008). Thecamoebians (testate amoebae) and foraminifera from three anchialine cenotes in Mexico: low salinity (1.5-4.5 psu) faunal transitions. *Journal of Foraminiferal Research* **38** (4), 305-317.

van Hengstum, P. J., Reinhardt, E. G., Medioli, F. S., and Gröcke, D. R. (2007). Exceptionally preserved Late Albian (Cretaceous) arcellaceans (thecamoebians) from the Dakota Formation near Lincoln, Nebraska, USA. *Journal of Foraminiferal Research* **37** (4), 300-308).

Ward, W.C. (2004). Geology of coastal islands, northeastern Yucatan Peninsula. In V. Leonard and T. Quinn (Eds.), *Geology and Hydrogeology of Carbonate Islands* (275-300), Neatherlands, Amsterdam: Elsevier Science.

Ward, W. C. and Brady, M. J. (1979). Strandline Sedimentation of Carbonate Grainstones, Upper Pleistocene, Yucatan Peninsula, Mexico. *American Association of Petroleum Geologists Bulletin* **63** (3), 362-369.

Wang, C., Lee, S.K., and Endfield, D. B. (2007). Impact of the Atlantic Warm Pool on the summer climate of the Western Hemisphere. *Journal of Climate* **20**, 5021-5039.

Wirth, K. and Barth, A. *Geochemical Instrumentation and Analysis: X-Ray Fluorescence (XRF)*. Retrieved from http://serc.carleton.edu/research_education/geochemsheets/techniques/XRF.html

7.0 FIGURE CAPTIONS

Figure 1 – Map of the study area (Yax Chen Cave, Yucatan Peninsula, MX) and seasonal migration pattern of the ITCZ (Intertropical Convergence Zone). Climate in the Yucatan Peninsula is predominantly controlled by the seasonal migration patterns of the ITCZ (Intertropical Convergence Zone) represented by the blue solid line. During summer months (March/April-October/November), the ITCZ moves northward to the Yucatan Peninsula bringing heavy precipitation and migrates south during the winter months (October/November-March/April).

Figure 2 – Summary of sedimentological and hydrological processes that affect Yucatan coastal aquifers. This illustrative diagram is an updated version adapted from the original figure published in van Hengstum et al (2010).

Figure 3 – (Top) Cave physiography of Yax Chen cave illustrating the main cave passages as well as the surrounding vegetation. Yax Chen extends to roughly 2.7km of the Ox Bel Ha network in Yucatan Peninsula of Mexico and encompasses around 8 collapsed sinkholes (cenotes) Yax Chen, Tarpon 1 and 2, L-Shaped, ISOD 1 and 2, Luna, and Gemini. The red dots indicate an approximate location of where the cores were collected along the main line. Sediment trap station locations for microfossil analysis is represented by the grey-yellow dots. The main entrance is cenote Yax Chen which is located in the Mayan tropical rainforest in close proximity to the Caribbean Sea. (Bottom) Cross sectional profile illustrating the high gradient of the Yax Chen cave passage and the relative position of the halocline in relation to where the cores were collected (red dots). Modified from Collins et al (2015b, Fig. 5).

Figure 4 – Salinity profiles of Arizona and Lil Chen showing a stepped halocline in Yax Chen Cave from Kovacs et al. (2017a). Data collected using handheld Hydrolab CTD MAS5 via SCUBA.

Figure 5 – Salinity calibration curve using raw Cl^- counts from various types of sediment found in cores collected around the Yucatan Peninsula and instrumental salinity in core locations. Data obtained from McNeill-Jewer et al. (submitted).

Figure 6 – Age-depth models created using CLAM 2.0 package for R-Studio using the radiocarbon dates obtained from each core. The black lines indicate an average weighted age at a given depth. The grey represents a 95 percent confidence interval of a given age and depth. The blue horizontal lines are indicative of calibrated ages of the organic sediment samples collected in each core. The red lines where applicable, illustrate dates that have been removed from the curve due to age reversals caused by potential sampling errors.

Figure 7A – Correlation of high resolution 200µm µXRF data (Cl, K, T, and Fe) and microfossil (foraminifera and arcellacean) results for C2 and C33. Lithological facies are illustrated in the optical image provided by the ITRAX core scanner. Radiocarbon sampling and corresponding ages are provided in cal. yr BP.

Figure 7B – Correlation of high resolution 200µm µXRF data (Cl, K, T, and Fe) and microfossil (foraminifera and arcellacean) results for C37 and C58. Lithological facies are illustrated in the optical image provided by the ITRAX core scanner. Radiocarbon sampling and corresponding ages are provided in cal. yr BP.

Figure 8 – Microfossil results from Yax Chen sediment trap stations for May-December 2016 period.

Figure 9 – Cross plots illustrating the relationship between the average relative abundances of *Elphidium* spp. collected from C2, C33, C37, and C58 and Cl^- counts obtained from the ITRAX XRF core scanner. The grey dotted line represents the overall global trend showing the positive relationship between *Elphidium* spp. and Cl^-.

Figure 10 – Cross plot showing the direct relationship between Cl^- and the detrital elements (K, Ti, and Fe) which are often used as proxies to measure weathering/terrigenous run off. A logarithmic best-curve fit was applied to achieve optimal R-squared values.

Figure 11 – Cl^- core correlation between C2 (blue), C33 (orange), C37 (grey), and C58 (yellow) plotted on the same scale. There is an overall freshening upward trend in C2, C33 and C37 as indicated by decreasing Cl^-. C2 and C33 which were collected at similar depths show a strong correlation in salinity changes in the meteoric WM with a few offsets related to dating errors and cave morphology (Figure 3). C37 and C58 which were collected at relatively similar depths have the greatest variability due to their close proximity to the halocline. Both C37 and C58 correlate well from 450 AD until ~1250 AD when the two Cl^- begin to diverge. C37 continues to show a decreasing trend in salinity and while C58 has an increasing salinity up core. This is related to I) the depth of where C58 was collected (at the halocline, Figure 3) and II) possibility of coastal plugging where the halocline has relatively stayed in the same position.

Figure 12 – Hydrologic response to wet and dry periods in Yax Chen Cave. Under wetter conditions, more mixing occurs due to increased flow in the meteoric WM resulting into higher salinity. During drier conditions, the groundwater is more stratified as a result of lower flow and mixing in the meteoric WM resulting to lower salinities. The relative position of the halocline moves up/down in response to these wet and dry conditions.

The halocline is deeper during wetter conditions due to higher recharge in the meteoric WM and is shallower during drier periods.

Figure 13 – Correlation of the climate records collected from caves and surface lakes from Mexico, Venezuela, Belize, and Guatemala. Major Classical Maya events including droughts and abandonments are highlighted in yellow and divided into the Post-Classical Abandonment, Medieval Warm Period, the Terminal Classic, and the Mayan Hiatus (Beach et al., 2016; Stahle et al., 2016; Douglas et al., 2014; Kennett et al., 2012; Hodell et al., 2005; Haug et al., 2001).

8.0 FIGURES

Figure 1

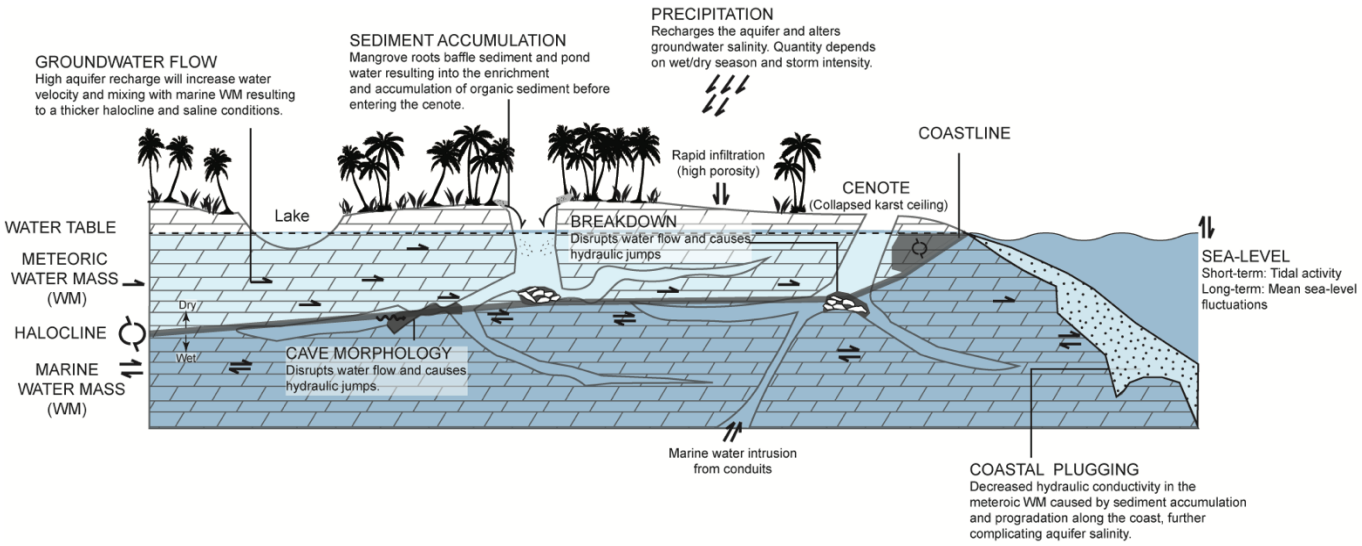
GROUNDWATER FLOW
High aquifer recharge will increase water velocity and mixing with marine WM resulting to a thicker halocline and saline conditions.
SEDIMENT ACCUMULATION
Mangrove roots baffle sediment and pond water resulting into the enrichment and accumulation of organic sediment before entering the cenote.
PRECIPITATION
Recharges the aquifer and alters groundwater salinity. Quantity depends on wet/dry season and storm intensity.
COASTLINE
Rapid infiltration (high porosity)
CENOTE
(Collapsed karst ceiling)
WATER TABLE
Lake
BREAKDOWN
Disrupts water flow and causes hydraulic jumps
METEORIC WATER MASS (WM)
HALOCLINE
MARINE WATER MASS (WM)
Dry
Wet
CAVE MORPHOLOGY
Disrupts water flow and causes hydraulic jumps.
SEA-LEVEL
Short-term: Tidal activity
Long-term: Mean sea-level fluctuations
Marine water intrusion from conduits
COASTAL PLUGGING
Decreased hydraulic conductivity in the meteroic WM caused by sediment accumulation and progradation along the coast, further complicating aquifer salinity.

Figure 2

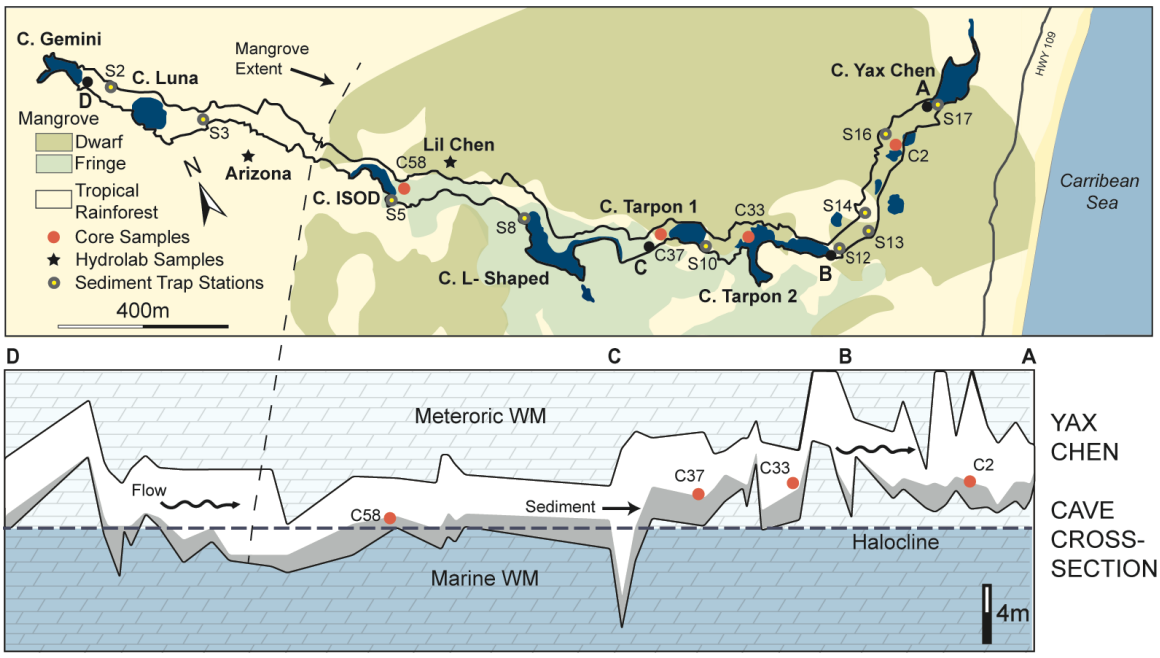
C. Gemini
S2
C. Luna
D
Mangrove
Dwarf
Fringe
Tropical
Rainforest
Core Samples
Hydrolab Samples
Sediment Trap Stations
400m
S3
Arizona
Mangrove
Extent
C58
Lil Chen
C. ISOD
S5
S8
C. L- Shaped
C. Tarpon 1
C37
S10
C33
C
B
C. Tarpon 2
S14
S13
S12
S16
C2
C. Yax Chen
A
S17
HWY 109
Carribean
Sea
D
C
B
A
Meteoric WM
Flow
C58
Sediment
C37
C33
C2
Halocline
Marine WM
4m
YAX
CHEN
CAVE
CROSS-
SECTION

Figure 3

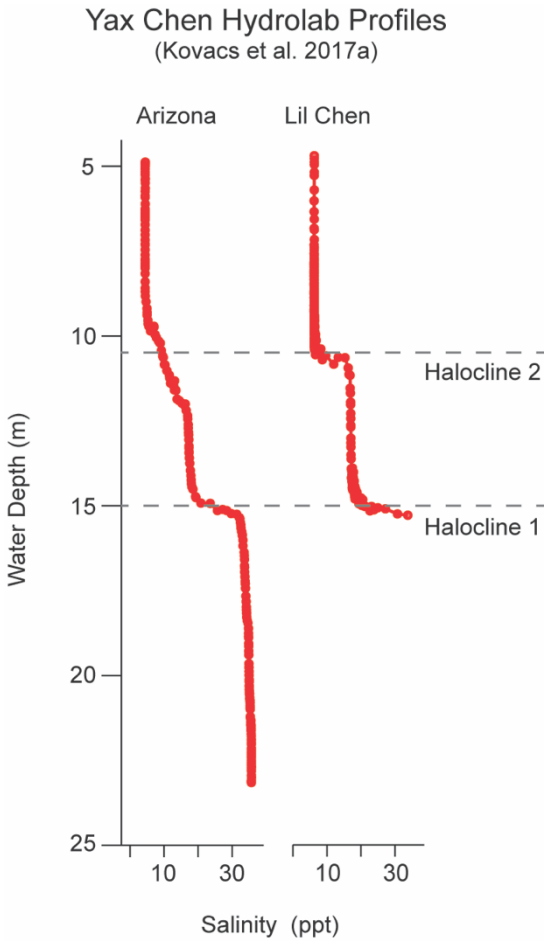
Yax Chen Hydrolab Profiles
(Kovacs et al. 2017a)
Arizona
Lil Chen
5
10
15
20
25
Water Depth (m)
Halocline 2
Halocline 1
10
30
10
30
Salinity (ppt)

Figure 4

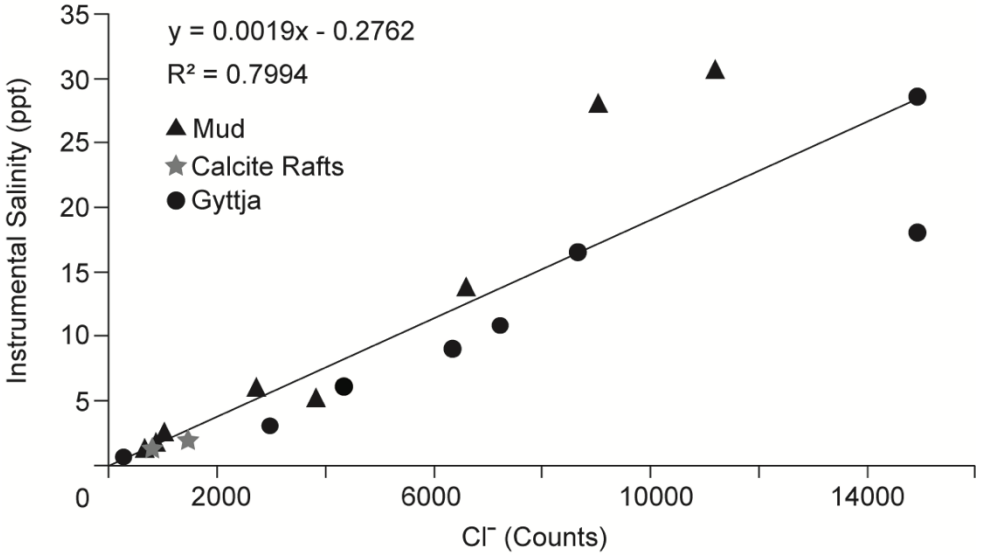
y = 0.0019x - 0.2762
R² = 0.7994
Mud
Calcite Rafts
Gyttja
Instrumental Salinity (ppt)
Cl⁻ (Counts)
0
2000
6000
10000
14000
5
10
15
20
25
30
35

Figure 5

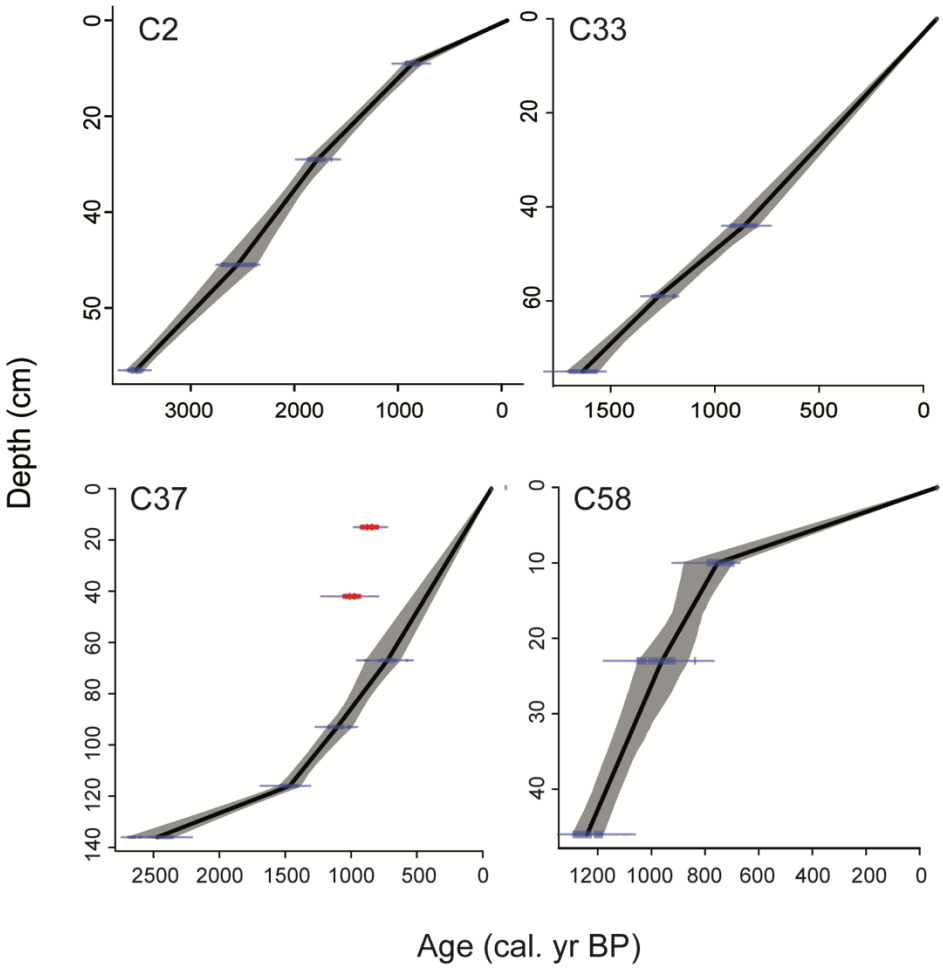
C2
C33
C37
C58
Depth (cm)
Age (cal. yr BP)
0
20
40
50
60
80
100
120
140
10
30
3000
2000
1000
1500
500
2500
1200
800
600
400
200

Figure 6

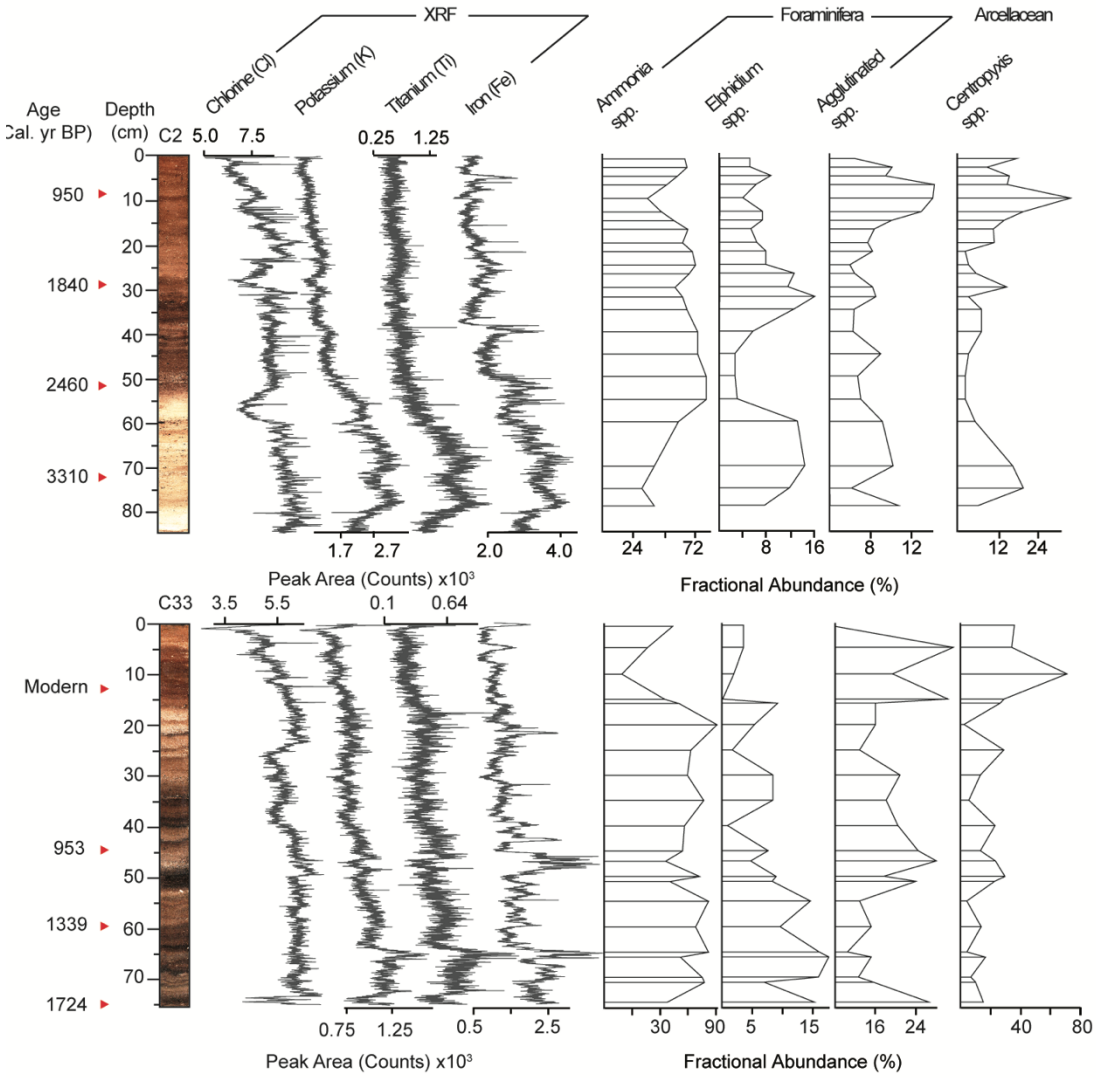
XRF
Foraminifera
Arcellacean
Chlorine (Cl)
Potassium (K)
Titanium (Ti)
Iron (Fe)
Ammonia spp.
Elphidium spp.
Agglutinated spp.
Centropyxis spp.
Age Cal. yr BP)
Depth (cm)
C2
5.0 7.5
0.25 1.25
950
1840
2460
3310
1.7 2.7
2.0 4.0
24 72
8 16
8 12
12 24
Peak Area (Counts) x10³
Fractional Abundance (%)
C33
3.5 5.5
0.1 0.64
Modern
953
1339
1724
0.75 1.25
0.5 2.5
30 90
5 15
16 24
40 80
Peak Area (Counts) x10³
Fractional Abundance (%)

Figure 7A

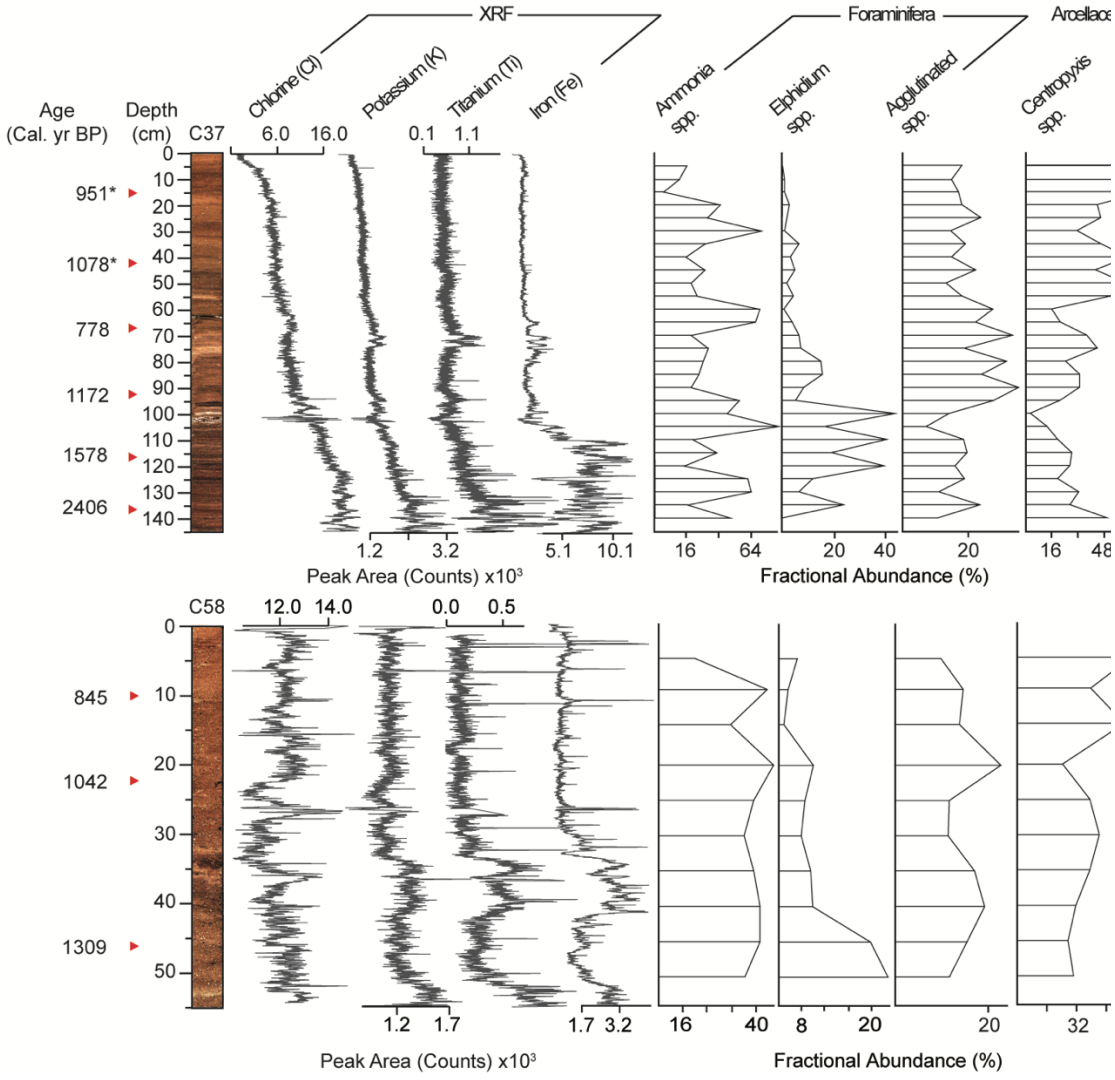
XRF
Foraminifera
Chlorine (Cl)
Potassium (K)
Titanium (Ti)
Iron (Fe)
Ammonia spp.
Elphidium spp.
Agglutinated spp.
Age (Cal. yr BP)
Depth (cm)
C37
6.0 16.0
0.1 1.1
951*
1078*
778
1172
1578
2406
1.2 3.2
5.1 10.1
16 64
20 40
20
16 48
Peak Area (Counts) x10³
Fractional Abundance (%)
C58
12.0 14.0
0.0 0.5
845
1042
1309
1.2 1.7
1.7 3.2
16 40
8 20
20
32
Peak Area (Counts) x10³
Fractional Abundance (%)

Figure 7B

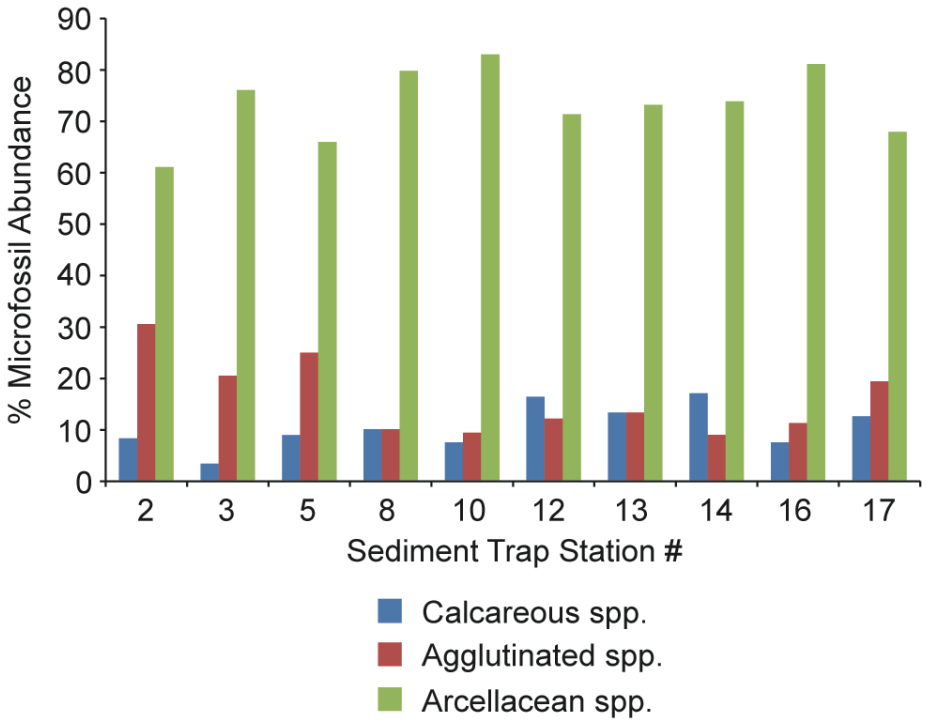
% Microfossil Abundance
90
80
70
60
50
40
30
20
10
0
2
3
5
8
10
12
13
14
16
17
Sediment Trap Station #
Calcareous spp.
Agglutinated spp.
Arcellacean spp.

Figure 8

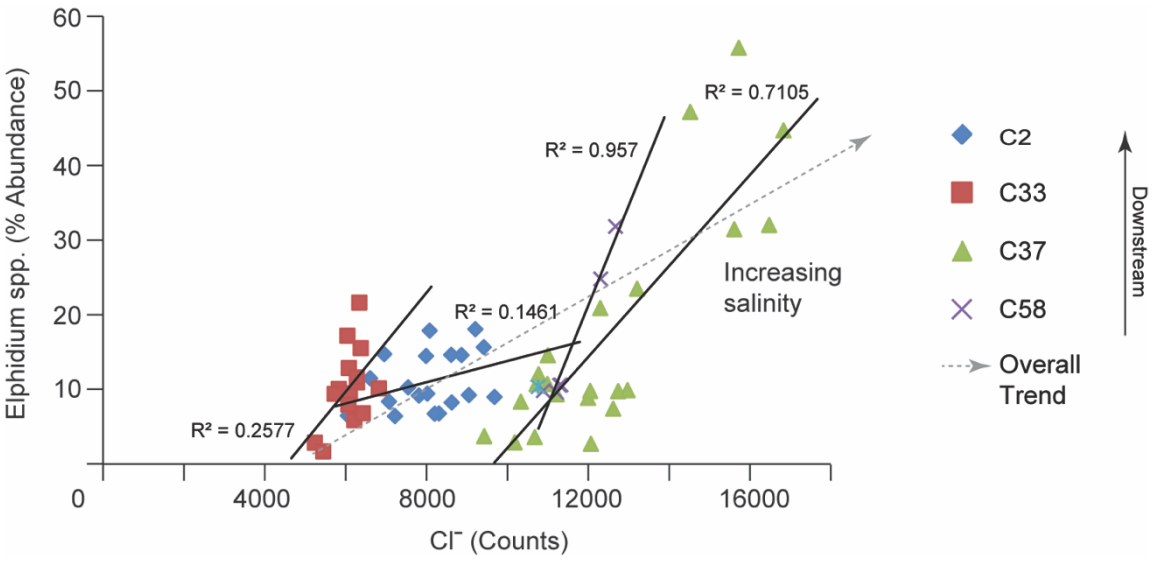
Elphidium spp. (% Abundance)
60
50
40
30
20
10
0
4000
8000
12000
16000
Cl⁻ (Counts)
R² = 0.2577
R² = 0.1461
R² = 0.957
R² = 0.7105
Increasing salinity
C2
C33
C37
C58
Overall Trend
Downstream

Figure 9

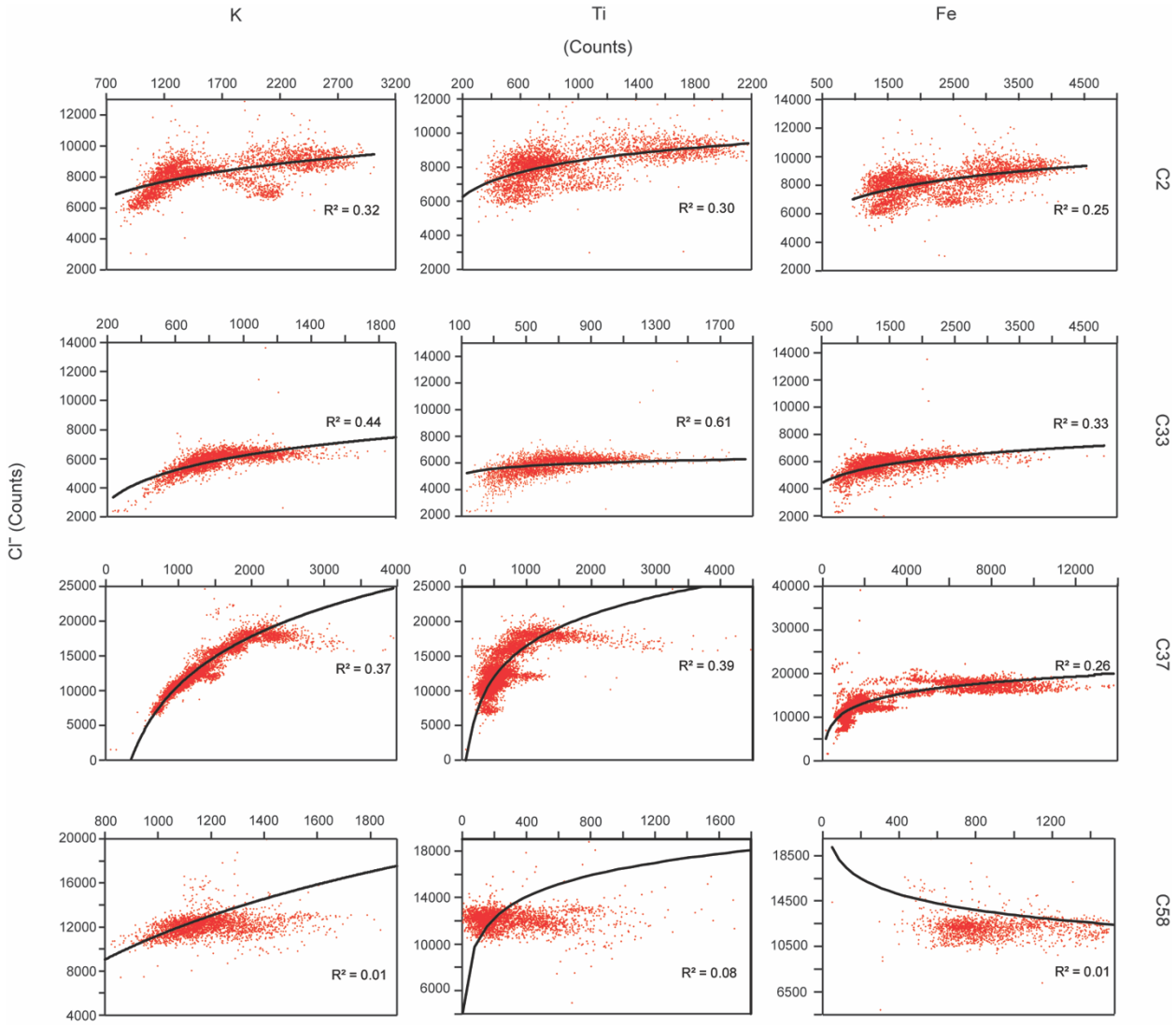
K
Ti
Fe
(Counts)
Cl⁻ (Counts)
C2
C33
C37
C58
R² = 0.32
R² = 0.30
R² = 0.25
R² = 0.44
R² = 0.61
R² = 0.33
R² = 0.37
R² = 0.39
R² = 0.26
R² = 0.01
R² = 0.08
R² = 0.01

Figure 10

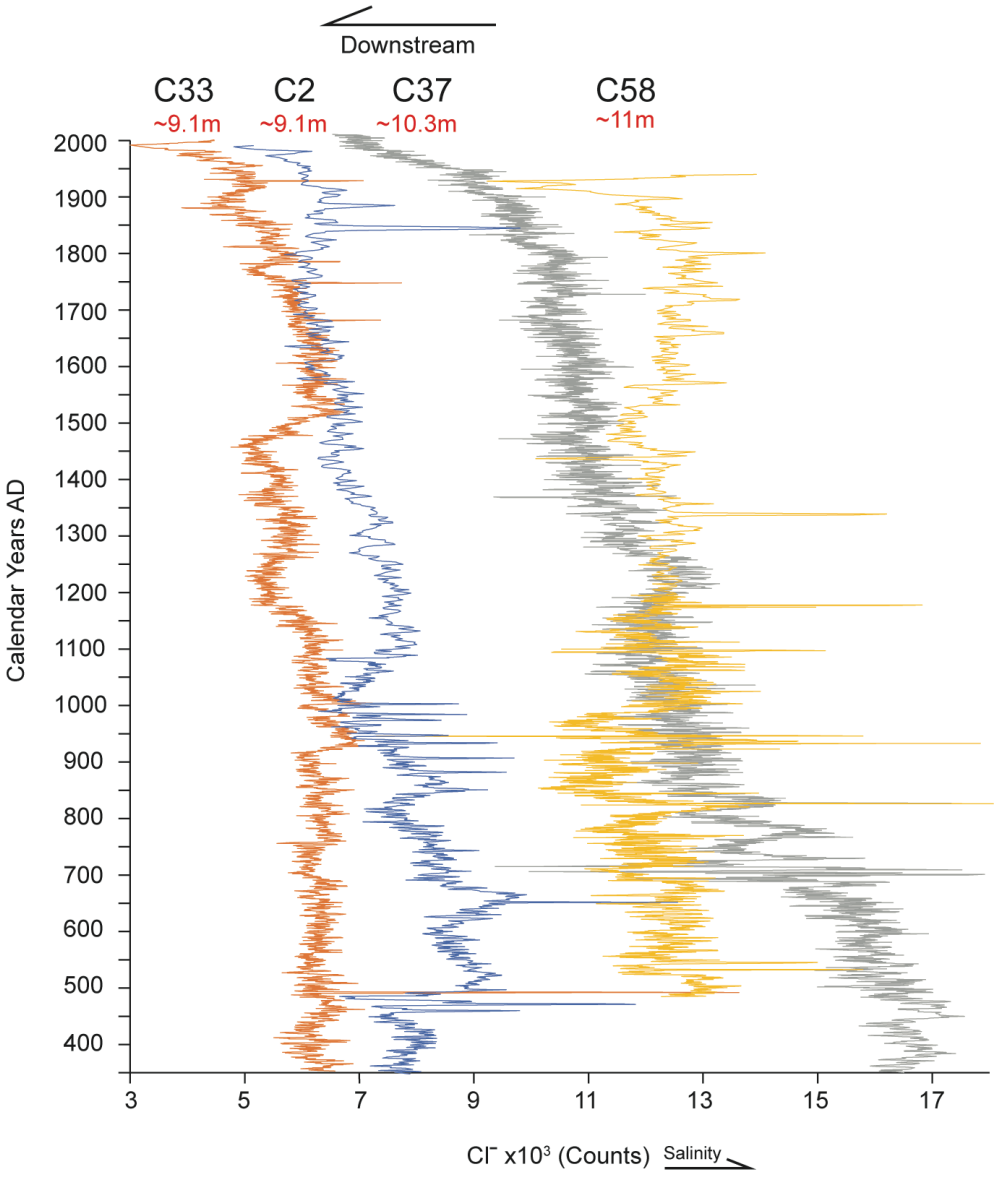
Downstream
C33
~9.1m
C2
~9.1m
C37
~10.3m
C58
~11m
Calendar Years AD
2000
1900
1800
1700
1600
1500
1400
1300
1200
1100
1000
900
800
700
600
500
400
3
5
7
9
11
13
15
17
Cl⁻ x10³ (Counts)
Salinity

Figure 11

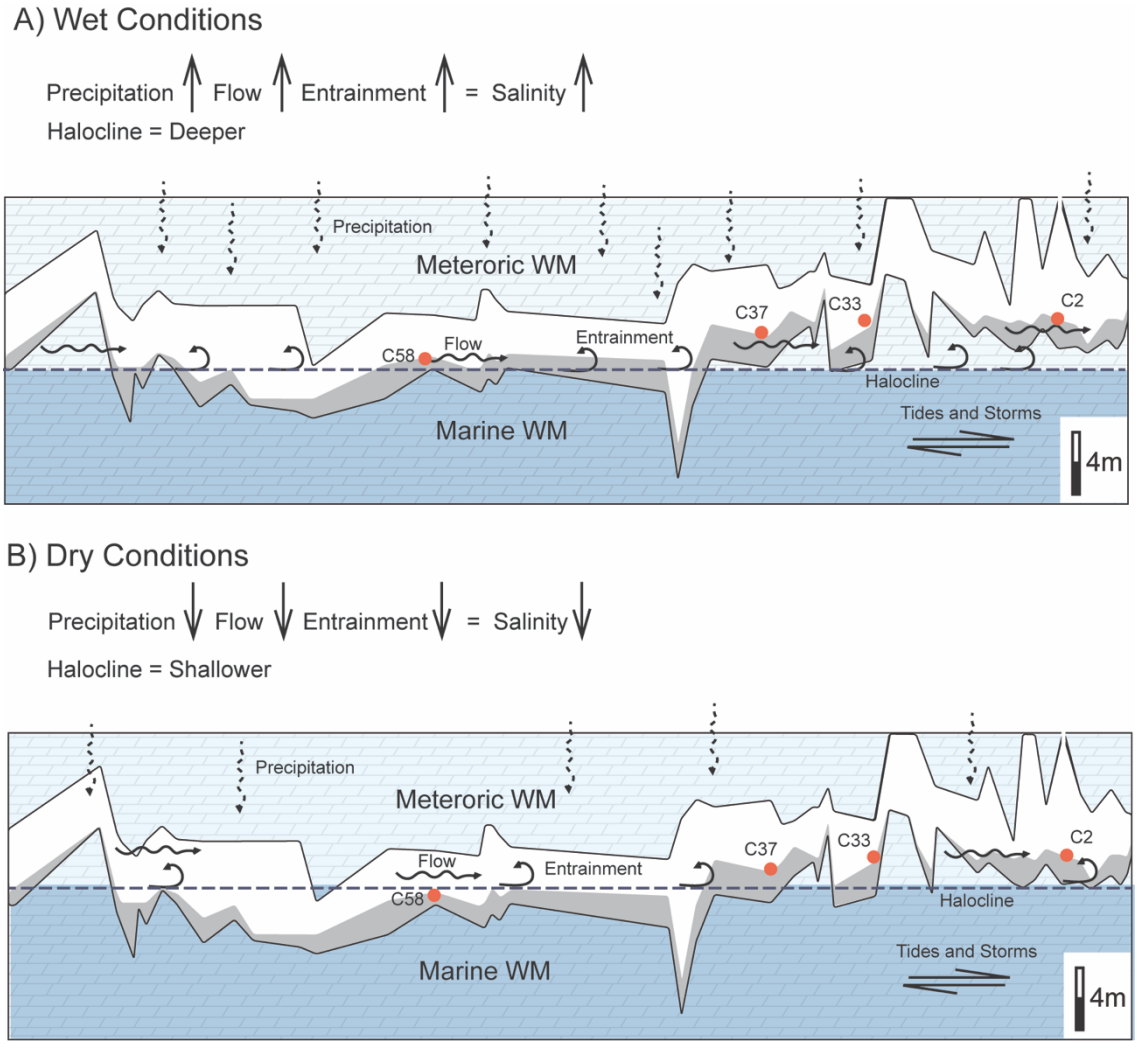
A) Wet Conditions
Precipitation
Flow
Entrainment
= Salinity
Halocline = Deeper
Precipitation
Meteroric WM
C58
Flow
Entrainment
C37
C33
C2
Halocline
Tides and Storms
Marine WM
4m
B) Dry Conditions
Precipitation
Flow
Entrainment
= Salinity
Halocline = Shallower
Precipitation
Meteroric WM
Flow
C58
Entrainment
C37
C33
C2
Halocline
Tides and Storms
Marine WM
4m

Figure 12

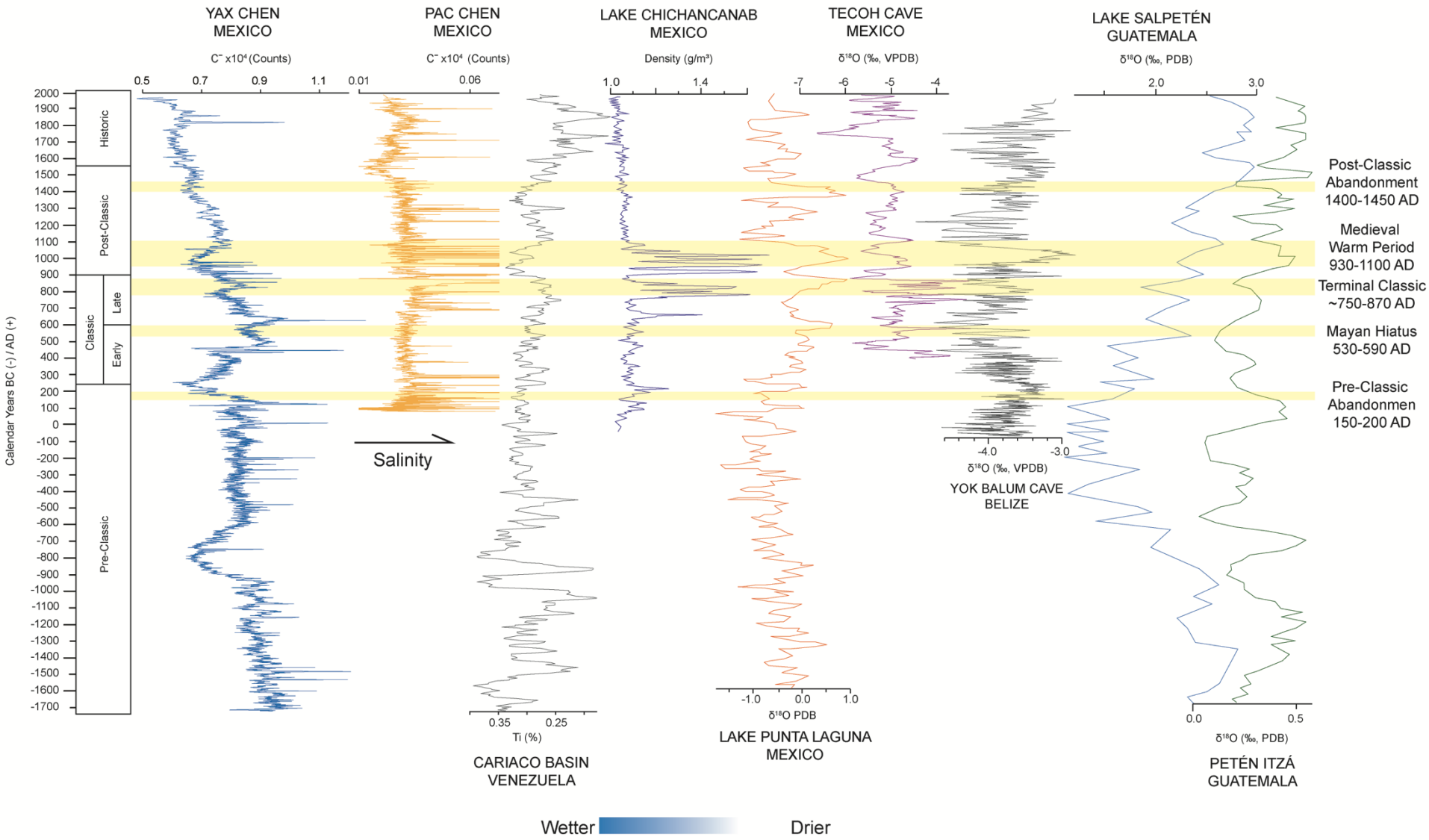
YAX CHEN
MEXICO
C⁻ x10⁴ (Counts)
PAC CHEN
MEXICO
C⁻ x10⁴ (Counts)
LAKE CHICHANCANAB
MEXICO
Density (g/m³)
TECOH CAVE
MEXICO
δ¹⁸O (‰, VPDB)
LAKE SALPETÉN
GUATEMALA
δ¹⁸O (‰, PDB)
Calendar Years BC (-) / AD (+)
Historic
Post-Classic
Classic
Late
Early
Pre-Classic
Salinity
Post-Classic
Abandonment
1400-1450 AD
Medieval
Warm Period
930-1100 AD
Terminal Classic
~750-870 AD
Mayan Hiatus
530-590 AD
Pre-Classic
Abandonmen
150-200 AD
δ¹⁸O (‰, VPDB)
YOK BALUM CAVE
BELIZE
Ti (%)
CARIACO BASIN
VENEZUELA
δ¹⁸O PDB
LAKE PUNTA LAGUNA
MEXICO
δ¹⁸O (‰, PDB)
PETÉN ITZÁ
GUATEMALA
Wetter
Drier

Figure 13

9.0 TABLES

TABLE 1 – Radiocarbon dates obtained from five cores collected in Yax Chen cave. The Laboratory codes OS-XXXXX were processed by Beta Analytic Laboratory in Gabriel et al. (2008) and codes with the prefix D-AMS-XXXXXX were processed by DirectAMS. The calibrated years BP were computed using Clam 2.2 (Blaauw, 2010) software package for Age-Depth modeling in R-Studio (version 1.1.383). (*) denotes ^{14}C that were contaminated and subsequently removed for further analysis.

CORE	LABORATORY CODE	CORE DEPTH (cm)	MATERIAL DATED	CONVENTIONAL RADIOCARBON AGE (^{14}C yr BP)	CALENDAR AGE (2σ) (cal yr BP)
C2-01	Beta-257280	9-10	OM	950 +/- 40	776-3486
C2-02	Beta-257281	29-30	OM	1840 ± 40	1696-1874
C2-03	Beta-257282	51-52	OM	2460 ± 40	2362-2618
C2-04	OS-74418	73-74	OM	3310 ± 30	3466-3618
C33-05	D-AMS 008975	12-12.5	OM	MODERN	MODERN
C33-01*	D-AMS 008367	18-18.5	OM	725 ± 26	652-699
C33-02	D-AMS 008366	44-44.5	OM	953 ± 26	796-885
C33-03	D-AMS 008368	59-59.5	OM	1339 ± 27	1239-1303
C33-04	D-AMS 008369	75-75.5	OM	1724 ± 28	1564-1701
C37-01	D-AMS 019659	15-16	OM	951 ± 32	795-926
C37-02	D-AMS 019660	42-43	OM	1078 ± 39	930-1059
C37-03*	D-AMS 019661	67-68	OM	778 ± 61	647-799
C37-04	D-AMS 019662	93-94	OM	1172 ± 27	1050-1179
C37-05	D-AMS 019663	116-117	OM	1578 ± 34	1398-1543
C37-06	D-AMS 019664	136-137	OM	2406 ± 40	2346-2517
C58-01	D-AMS 019665	10-11	OM	845 ± 27	691-794
C58-02	D-AMS 019666	23-24	OM	1042 ± 39	910-1013
C58-03*	D-AMS 019667	36-37	OM	827 ± 34	683-792
C58-04	D-AMS 019668	46-47	OM	1309 ± 25	1228-1291